U-Pb geochronology and paleo-magnetism of the Westerberg sill, Kaapvaal Craton – support for a coherent Kaapvaal-Pilbara block (Vaalbara)

Tobias Christoph Kampmann

Dissertations in Geology at Lund University,
Master's thesis, no 313
(45 hp/ECTS credits)

Department of Geology
Lund University
2012

U-Pb geochronology and paleomagnetism of the Westerberg sill, Kaapvaal Craton - support for a coherent Kaapvaal-Pilbara block (Vaalbara)

Master's thesis

Tobias Christoph Kampmann

Department of Geology
Lund University
2012

Contents

Cover Picture: Drill hole for paleomagnetism in an exposure of the Westerberg intrusion along the banks of Orange River, South Africa.

U-Pb geochronology and paleomagnetism of the Westerberg sill, Kaapvaal Craton - support for a coherent Kaapvaal-Pilbara block (Vaalbara)

TOBIAS CHRISTOPH KAMPMANN

Kampmann, T.C., 2012: U-Pb geochronology and paleomagnetism of the Westerberg sill, Kaapvaal Craton - support for a coherent Kaapvaal-Pilbara block (Vaalbara). *Dissertations in Geology at Lund University*, No. 313, 32 pp. 45 hp (45 ECTS credits).

Abstract: Well-constrained paleopoles combined with precise geochronology provide important information for obtaining robust paleoreconstructions and can reveal the history of supercontinent formation and break-up through time. These techniques are used in the attempt to complete the polar wander paths of Archean and Proterozoic cratons. Paleomagnetic data of intrusive bodies are particularly useful to this end. A new baddeleyite U-Pb age of 2442 ± 5 Ma for the intracratonic Westerberg sill within the Kaapvaal Craton of southern Africa falls in the centre of a ca. 450 Ma gap, between 2.66 and 2.22 Ga. No paleopoles have been obtained previously for Kaapvaal over this time interval. The igneous unit intrudes the banded iron formations of the Kuruman Formation, Transvaal Supergroup. Its key position in close proximity to the south-western boundary of the craton potentially provides an excellent record of its relationship to other cratons. A comparison with the coeval Woongarra igneous unit on the Pilbara Craton of Western Australia suggests a synchronous volcanic event, possibly forming a large igneous province on the joined landmasses of Kaapvaal and Pilbara. Vaalbara would represent the oldest known assemblage of cratons. The virtual geomagnetic pole obtained for Kaapvaal (52.2° N, 93.5° E, dp = 6.2° and dm = 11.6°) falls well within the existing reconstruction of the craton's polar wander path. Furthermore, combined with a coeval Pilbara pole, it allows for reconstructions of Vaalbara that place Pilbara to the north of Kaapvaal.

Keywords: Kaapvaal, Pilbara, Vaalbara, baddeleyite, U-Pb geochronology, paleomagnetism, continental reconstruction

Supervisors: Ulf Söderlund (Lund University), Michiel De Kock (University of Johannesburg)

Subject: Bedrock Geology

Tobias Christoph Kampmann, Department of Geology, Lund University, Sölvegatan 12, SE-223 62 Lund, Sweden. E-mail: tobias.kampmann@onlinehome.de

U-Pb geokronologi och paleomagnetismstudier av Westerbergdiabastäcket, Kaapvaalkratonen: stöd för ett sammanhängande Kaapvaal-Pilbara-block (Vaalbara)

TOBIAS CHRISTOPH KAMPMANN

Kampmann, T.C., 2012: U-Pb geokronologi och paleomagnetismstudier av Westerbergdiabastäcket, Kaapvaalkratonen: stöd för ett sammanhängande Kaapvaal-Pilbara-block (Vaalbara). *Examensarbeten i geologi vid Lunds universitet*, Nr. 313, 32 sid. 45 hp.

Sammanfattning: För att erhålla kompletta polvandringskurvor för arkeiska och proterozoiska kratoner krävs robust paleomagnetisk data från bergarter vars åldrar är välbestämda. Dessa tekniker ger oss möjlighet att förstå hur kratoner som idag är vitt utspridda en gång satt ihop relativt varandra. I denna studie presenteras en exakt U-Pb-ålder på 2442 ± 5 Ma (miljoner år) för ett diabastäcke, "the Westerberg sill", i Kaapvaalkratonen. Åldern för diabastäcket faller inom en period (2660 till 2220 Ma) inom vilken motsvarande data helt saknas. Westerbergdiabasen intruderar järnrika sediment ("banded iron formations") tillhörande Kurumanformationen som har en strategisk position nära Kaapvaalkratonens sydvästra kant. Därmed kan diabastäcket ha bildats i samband med uppsprickning av Kaapvaal och en annan kontinent, vilket innebär att dess ålder kombinerat med dess paleomagnetiska signatur kan användas för att få information om hur Kaapvaalkratonen rört sig relativt andra kratoner under tidspannet senarkeisk till tidigpaleoproterozoisk tid. En jämförelse med motsvarande data av en likåldrig magmatisk svit kallad Woongarra, som återfinns i Pilbarakratonen (nuvarande NW Australien), bekräftar att Kaapvaal och Pilbara en gång satt ihop i en större landmassa känd som Vaalbara. Den erhållna virtuella geomagnetiska polen (52.2° N, 93.5° E, dp = 6.2° och dm = 11.6°) för Westerbergdiabasen stämmer överens med existerande polvandringsdata från äldre och yngre undersökta enheter i Kaapvaal. Vidare är resultaten förenliga med den tidigare uppfattningen att Pilbara en gång var beläget norr om nuvarande Kaapvaalkratonen.

Nyckelord: Kaapvaal, Pilbara, Vaalbara, baddeleyit, U-Pb geokronologi, paleomagnetism, kontinentrekonstruktion

Tobias Christoph Kampmann, Geologiska institutionen, Lunds universitet, Sölvegatan 12, 223 62 Lund, Sverige.
E-post: tobias.kampmann@onlinehome.de

1 Introduction

The onset of 'modern' plate tectonics has been constrained recently to approximately 3.2 Ga (Næraa et al., 2012). However, the nature and mechanisms of the early tectonic movements of plates is a matter of debate due to the sparse geological record of Archean rocks. There are approximately 35 preserved fragments of Archean continental crust which are now distributed globally (Bleeker, 2003). One of the fundamental questions concerning late Archean continental arrangement is whether the existing continental crust was amalgamated into a single supercontinent (Kenorland) or into a few smaller supercratons (Superia, Sclavia and Vaalbara). The current lack of a continuous paleomagnetic record for the Archean and Paleoproterozoic prevents a full understanding of plate movements during these eras. However, it is thought to have occurred at higher rates of speed than today due to a steeper geothermal gradient (Moyen and van Hunen, 2012).

The combination of precise U-Pb geochronology and paleomagnetic investigations is a powerful approach in paleogeographic reconstruction. Tectonic kinematics are thought to be both associated with and triggered by increased magmatic activity. This often forms large igneous provinces (LIPs) which might extend over craton boundaries. Precise emplacement ages of those igneous units, together with information on latitudinal and relative longitudinal position, can be used to determine the so-called wander path history of a craton through geological time. In addition it can also be used for reconstructing interconnections with other cratons, the possible amalgamation of supercratons and their break-up. Results from recent studies (e.g. De Kock et al., 2009; Buchan et al., 2009; Evans and Halls, 2010) have had a large impact in the field of paleogeography, building on the understanding of the paleogeographic framework of the Archean and Proterozoic. Furthermore, an ancient connection between two cratons that are now separated and dispersed around the globe might be of significant economic interest. If there are, in fact, valuable deposits associated with a craton, they could thereby potentially be traced to another continent. This could result in a new approach to prospecting for resources.

The Kaapvaal Craton of southern Africa has long attracted the attention of research and is probably the most studied of all Archean cratons. This is partly due to the extraordinary preservation of >2.0 Ga old crustal features such as the Witwatersrand and Transvaal supergroups and the Bushveld Igneous Complex, as well as the large number of economically viable resource deposits associated with the craton. All previously published studies imply a complex history, with some placing constraints on the nature of early plate tectonics.

The most popular connection currently disputed regarding the Kaapvaal Craton during the Archean and Paleoproterozoic is with the Pilbara Craton of Western Australia. The assemblage of these two cratons (Vaalbara) was first proposed by Cheney et al. (1988). There has been a lively debate since on its existence, the configuration of the continents and the time frame from its amalgamation to its break-up. Indeed, confirmation of the Vaalbara hypothesis would establish it as the oldest supercraton in Earth history.

This study focuses on a U-Pb geochronology and paleomagnetism study of the Westerberg intrusion, an intracratonic igneous suite of the Kaapvaal Craton. The results obtained and their comparison with data from coeval units of Pilbara could lead to new conclusions regarding the reconstruction of Vaalbara and provide an important piece to the puzzle of continental and tectonic reconstruction during the Archean and Paleoproterozoic.

2 Geological setting

The Kaapvaal Craton can be divided into a 3.6 - 2.9 Ga old crustal basement, consisting of granitoid-greenstone units, and overlying 3.1 - 1.7 Ga sedimentary and volcanic sequences. Several basement terranes can be distinguished. According to Brandl et al. (2006) and Eglington and Armstrong (2004), the 3.6 - 2.9 Ga Witwatersrand Block in the eastern part of the craton represents the oldest terrane, with younger, accreted terranes to the north (Pietersburg Block, 3.2 - 2.8 Ga) and west (Kimberley Block, 2.9 - 2.6 Ga). Fig. 1 shows the general geological setting of Kaapvaal Craton in South Africa.

Sedimentation of the Dominion Group started at 3.1 Ga and was followed by uplift and erosion of the greenstone-granite basement (Bumby et al., 2011). Accumulation of the sediments of the Witwatersrand Supergroup commenced at ca. 3.1 Ga and terminated at about 2.7 Ga (McCarthy, 2006). The Dominion Group and Witwatersrand Supergroup are limited to the older Witwatersrand Block of the Kaapvaal Craton. Their deposition was followed by a period of extensive volcanism which resulted in the emplacement of the Ventersdorp Supergroup. This unit consists mainly of basaltic lavas reaching thicknesses of ca. 8 km (e.g. Van der Westhuizen et al., 2006). These extend through most of the Witwatersrand Block and into the younger Kimberley Block. After the Ventersdorp volcanism ceased, deposition of the Transvaal Supergroup commenced, formed by clastic and carbonate sedimentation as well as minor volcanic activity. A good age estimate for the onset of sedimentation is provided by a Vryburg formation lava (Griqualand West Basin) dated to 2642 ± 3 Ma using zircon Pb-Pb evaporation (Walraven and Martini, 1995). Deposition of the Transvaal Supergroup occurred in three separate basins; the Transvaal Basin on the Witwatersrand Block and the Griqualand West Basin on the Kimberley Block (both in South Africa), and the Kanye Basin (in Botswana). These basins share similar geological

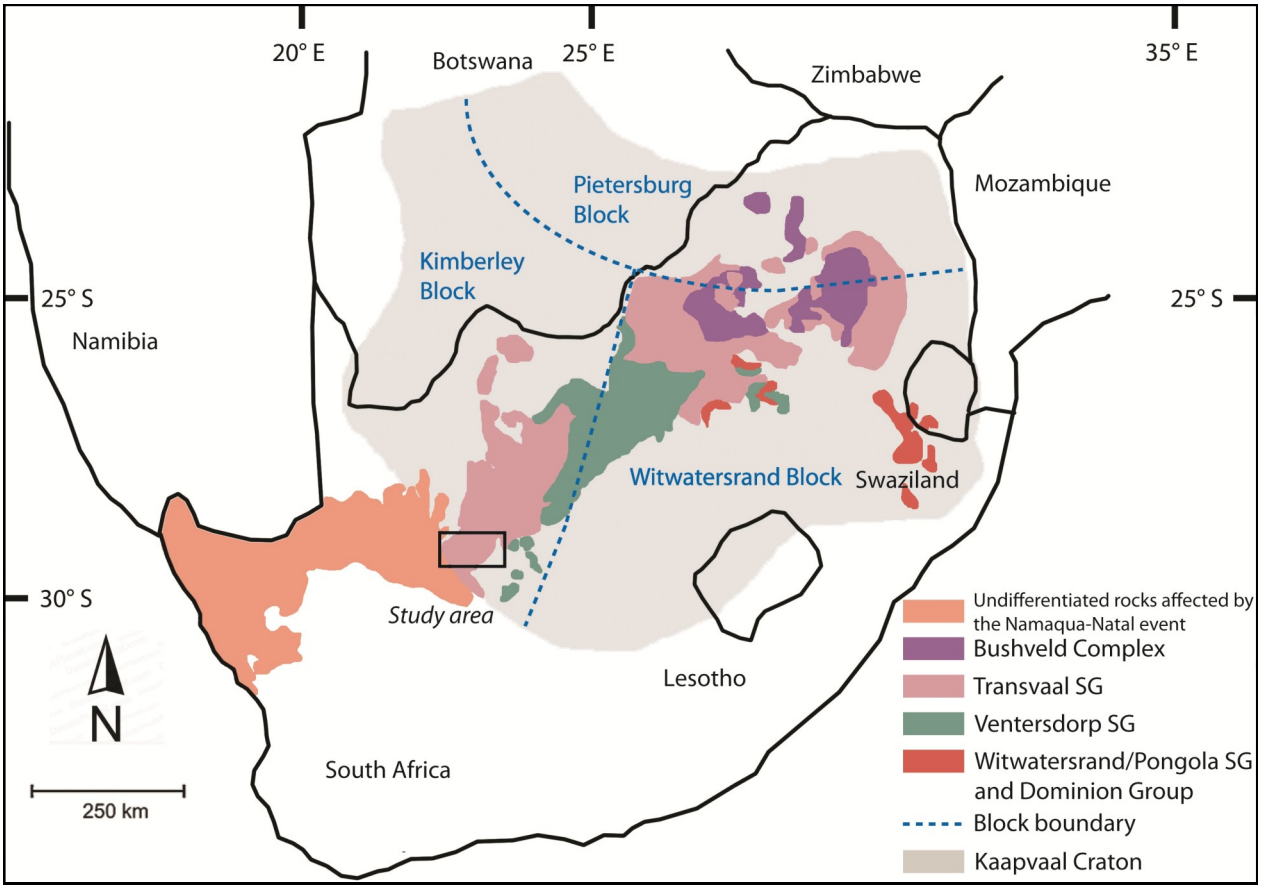

Fig. 1. Geological setting of Kaapvaal Craton units in South Africa. Outcrop distributions of the major >2.0 Ga units are shown, simplified after the geological map of South Africa (Keyser, 1997). Transvaal Supergroup successions of the Kanye Basin in Botswana are not shown. The schematic division into three tectonic blocks is based on Eglington and Armstrong (2004). Abbreviations in legend: met. prov. = metamorphic province, SG = Supergroup.

evolutions and sediment stratigraphies. Four major units can be distinguished. The protobasinal suite is restricted to the Transvaal Basin. It is superimposed by the Black Reef Formation which is found in both the Transvaal and Kanye basins. The carbonate to banded iron formation (BIF) platform successions (Chuniespoort, Ghaap and Taupone groups in the Transvaal, Griqualand West and Kanye basins respectively) and the overlying mixed clastic and chemical sediments (Pretoria, Postmasburg and Segwagwa groups) are widespread and common to all three basins (Eriksson et al. 2006). The Ghaap Group of the Griqualand West Basin also hosts the Westerberg intrusion, which is the focus of this study (Fig. 2).

The Ghaap Group consists of a sedimentary package of carbonates, overlying BIF and a series of mixed clastic and chemical sediments. It superimposes a regional unconformity that resulted from base level fall and tilting. Spatial reconstructions based on sedimentary facies assemblages show a gradual deepening of the sedimentary environment from the Prieska sub-basin in the southwest to the Ghaap Plateau sub-basin in the east-northeast. Two major transgressions at 2550 Ma and 2500 Ma resulted in a change to a more distal depositional environment with stratigraphic progression from platform carbonates over sub-tidal muds into BIFs (Eriksson et al., 2006). Successive units are the 2555 - 2516 Ma Campbell Rand Subgroup carbonates, the BIF deposits of the Kuruman Formation (~2500 Ma SHRIMP U-Pb ages by Trendall et al., 1995) and the BIF deposits of the Daniëlskuil Formation. Accumulation of the youngest mixed clastic and chemical Koegas Subgroup sediments represents the final regression of the epeiric sea off the Kaapvaal Craton. The unit has yet to be dated directly, but must predate the overlying igneous Ongeluk Formation with a Pb-Pb isochron age of 2222 ± 13 Ma (Cornell et al., 1996).

Deposition of the Transvaal sediments ended abruptly with the emplacement of the Bushveld Complex, which started with the extrusion of the felsic Rooiberg lavas at 2061 ± 2 Ma (Walraven, 1997). The magmatic activity culminated with the intrusion of the mafic-ultramafic Rustenburg Layered Suite, the largest known layered intrusion, which hosts enormous PGE- and Cr- ore reserves (Eales and Cawthorn, 1996). The emplacement of the Rustenburg Layered Suite is bracketed between a U-Pb baddeleyite age of 2057.7 ± 1.6 Ma (Olsson et al., 2010) and a U-Pb zircon age of 2054.4 ± 1.3 Ma (Scoates and Friedman, 2008).

At about 1.2 Ga, the Namaqua-Natal belt started to form by successive accretion of several terranes to the west of the craton. Collision with the Kaapvaal Craton continued to about 1.02 Ga (Eglington and

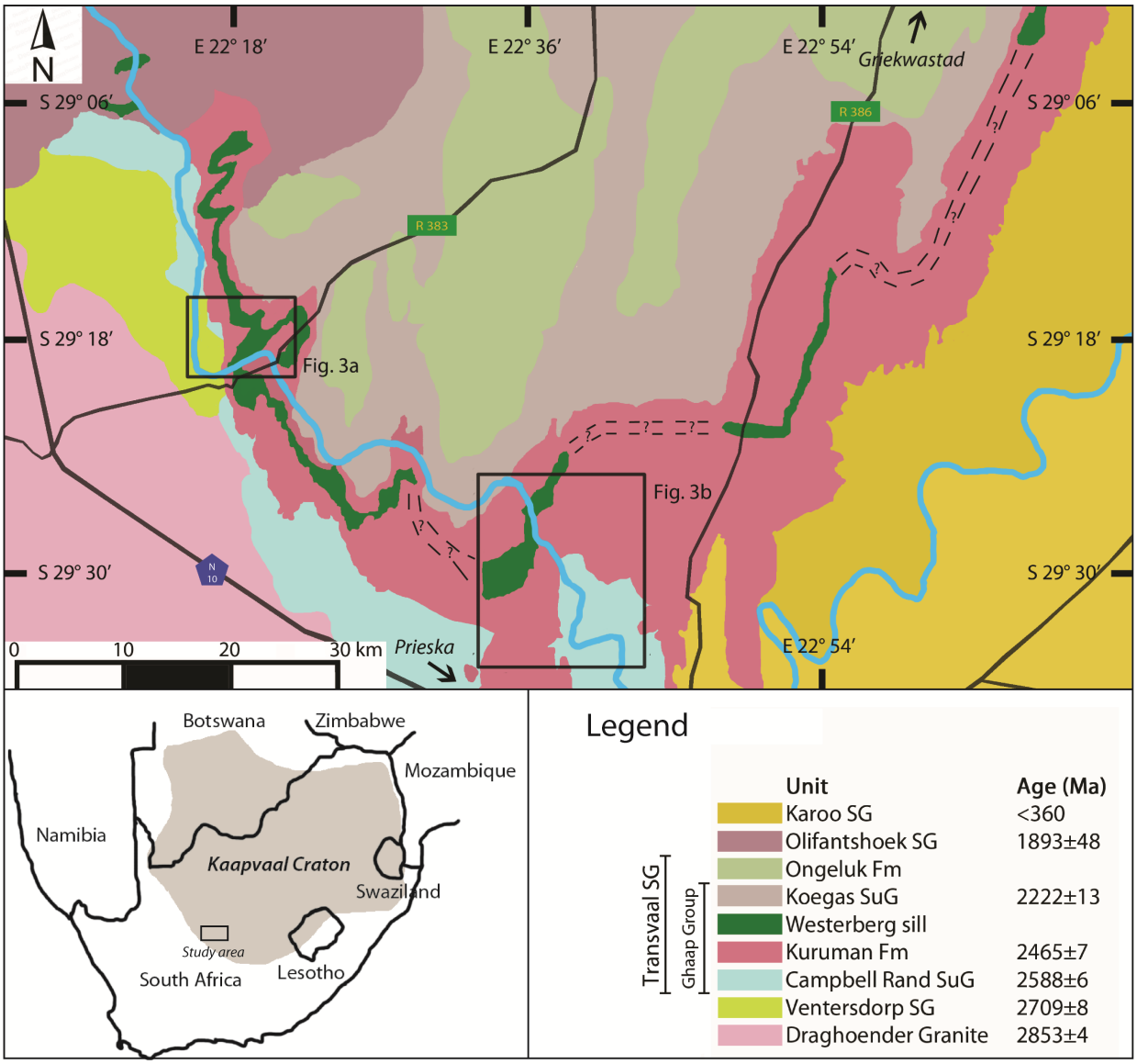

Fig. 2. Simplified geological map of the study area (see Fig. 1) after Malherbe and Moen (1996). The Westerberg sill was sampled for paleomagnetism at two locations, here shown by the black framed areas enlarged in Figure 3. Stippled lines between segments of the sill mark its assumed extent. Abbreviations in legend: SG= Supergroup, SuG= Subgroup, Fm= Formation.

Armstrong, 2004), resulting in orogeny and regional metamorphism.

3 The Westerberg intrusion

Field work was performed at two localities, one near the village of Westerberg (paleomagnetism sites TKWA, TKWB and TKWE) and the other near Naauwte farm (paleomagnetism sites TKWC and TWKD). Fig. 2 shows the Westerberg intrusion and Fig. 3 displays the two field localities.

The Westerberg sill intruded a region that was thoroughly reworked between 1.20 - 1.02 Ga during the Namaqua-Natal orogeny (Eglington, 2006). Extensive folding of the Transvaal stratigraphy, including the Kuruman Iron Formation and the Westerberg intrusion, is also evidence of a deformational event which could have been connected to a second, older orogeny. Folding resulted in a large synclinal structure which dominates the study area (Fig. 2). The fold axes trend predominantly north-south and also contain parasitic folds (De Kock, 2007). Fig. 4 is a stereographic determination of the fold axis using bedding measurements by Dreyer (1982). The resulting fold axis, with an azimuth of 19.1° and a plunge of 19.4°, is assumed herein to be representative of the Westerberg syncline. Folding related to this event is still recognizable in the 2.22 Ga Ongeluk Formation. However, it is absent in the oldest, 1.93 Ga Olifantshoek Supergroup successions, thereby indicating that the orogeny took place in the interval between these ages (De Kock, 2007).

The intrusive body has a varying overall thickness of 50 – 200 m and is composed of doleritic to gabbroic rock. Grain size is directly dependent on the proximity to the contact with the surrounding BIF

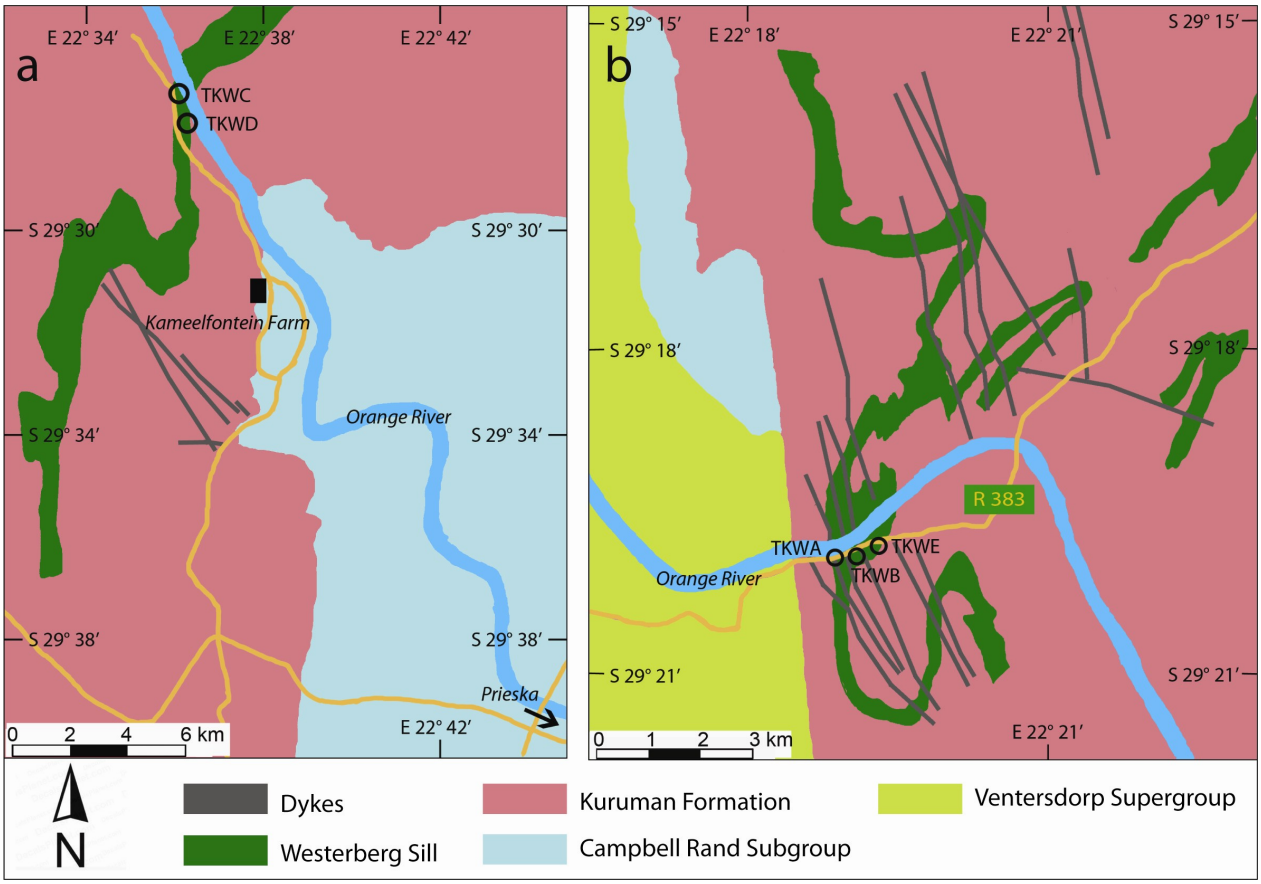

Fig. 3. Geological maps of the two study areas (see Fig. 2 for overview), including sites for paleomagnetic sampling. Simplified after Dreyer (1982).

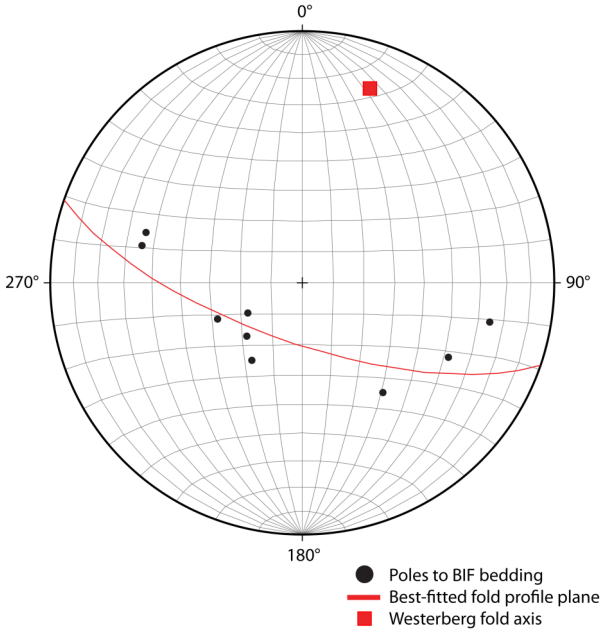

Fig. 4. Stereographic determination of the Westerberg fold axis using sedimentary bedding data from the Westerberg area (Fig. 3b) by Dreyer (1982). The resulting fold axis plunges 19.4° with an azimuth of 19.1°.

sediments, with a maximum of ca. 5 mm in the centre of the body. The hosting BIF sediments consist of alternating, parallel red and grey layers of varying thickness from 1 - 5 cm. The red colour results from high ferric iron content, whereas the grey layers contain Fe-poor shale and chert. The BIF shows clear evidence of thermal alteration up to ca. 0.5 m from the rock boundary, which is caused by thermal heat flux from the intrusion. However, preservation of the original sedimentary layering in the BIF indicates that the intrusion occurred at a stage when the sediments were already lithified (see Fig. 5).

Columnar jointing forming hexagonal pillars is clearly recognizable and especially well developed in proximity to the contact with the BIF host rock. This magmatic feature forms due to cooling which propagates from the contact zone to the host rock and perpendicular to the contact of the intrusion. In the Westerberg area the intrusion is divided into an upper part (ca. 50 m in thickness) and a lower part (ca. 100 m in thickness) with a section of ca. 50 m of BIF in between. Both dolerite branches have identical lithology. This suggests that they crystallized from magmas fed by a common dyke. The dolerite intrusion in the Westerberg area is cross-cut by dykes of younger magmatic generations. These are ca. 5 m in thickness, strike northwest to southeast (Fig. 3) and are more susceptible to weathering, forming topographic troughs in the landscape (Fig. 6).

Fig. 7 shows polarization microscopy photographs taken for illustration of the basic petrography of the Westerberg dolerite. The rock structure is isotropic throughout the whole unit and is especially visible due to the randomly oriented growth of porphy-

Fig. 5. Exposed margin of the intrusion and overlying BIF sediments. Note that the contact of the sill is parallel to the BIF bedding (bottom). The section of thermally altered BIF (middle) grades into unaltered BIF (top).

ritic pyroxene crystals in the central, coarser-grained part of the body. Sericitisation of plagioclase (Fig. 7a) is common, indicating a secondary influx of potassium -rich hydrothermal fluid. Chlorite is present, probably as the product of low-grade metamorphic alteration of mafic minerals (Fig. 7a). Magnetite is present throughout the groundmass as small, euhedral crystals of 0.1 - 0.3 mm in diameter. The outer surfaces of the crystals appear somewhat heterogeneous and might have been affected by the same hydrothermal fluid (Fig. 7b). Magnetite is the most probable carrier phase of primary magnetization. The small grain size and otherwise homogeneous appearance of the magnetite indicate that single-grain domains are predominant. These properties are conducive to recording remanent magnetization.

Although there have been several studies of the geology in the Koegas/Westerberg area, none have focussed particularly on the Westerberg intrusion. Dreyer (1982) categorizes the Westerberg dolerite intrusion as a sill but does not present any further evidence. Altermann and Hälbich (1990), on the other hand, state that the intrusion is a dyke-like body intruding at a low angle to the bedding of the host sediments. Again, not much evidence is provided for this claim. A classification of the intrusion of the Westerberg dolerite in relation to the host sediments is crucial for this study as it determines the bedding parameters used for tilt-correction of the primary magnetic components. As no foliation in the dolerite itself has been observed, the contact zone to the surrounding supracrustal BIFs was examined at several outcrops in the Westerberg and the Naauwte areas. No signs of angular discordance were observed (Fig. 5) and the angle between the BIF bedding and columnar joints of the intrusion appears to be 90° (Fig. 8).

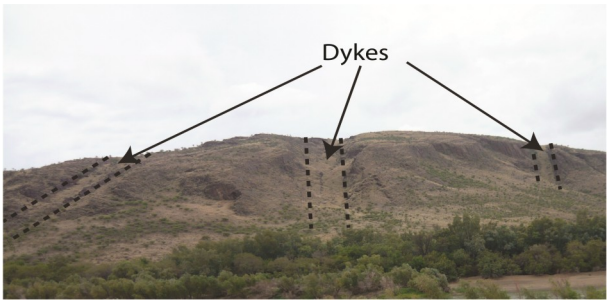

Fig. 6. Dykes intruding the Westerberg sill. Due to lower resistance to weathering these intrusions form troughs in the landscape.

For further corroboration, the columnar surface orientation of the distinct columnar jointing was measured at two sites, TKWA (Westerberg area) and TKWC (Naauwte area), and plotted on a stereonet. The pole to the great circle, defined by the calculated columnar surface poles, plots within the 95% confidence cone to the BIF bedding orientation pole (Fig. 9). Differences in orientation between the sites are due to the complex deformation of the study area as described previously (Fig. 3). Columnar joints develop perpendicular to the isotherms during cooling (Spry, 1962) and hence perpendicular to the emplacement of the subvolcanic intrusion. The columnar jointing test therefore confirms the assertion by Dreyer (1982) that the Westerberg intrusion was emplaced as a subvolcanic sill.

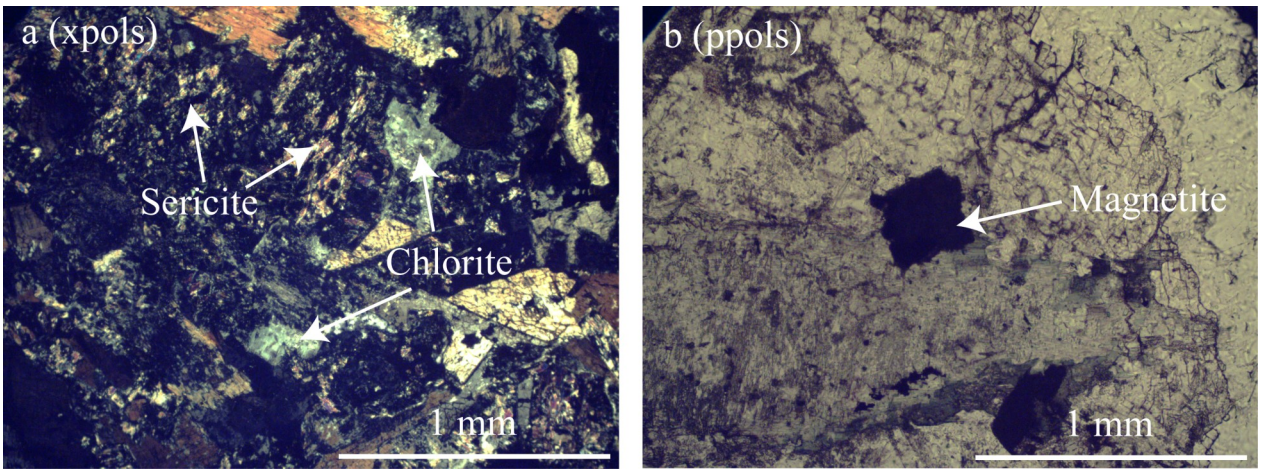

Fig. 7. Polarisation microphotographs of the coarse-grained part of the Westerberg dolerite.

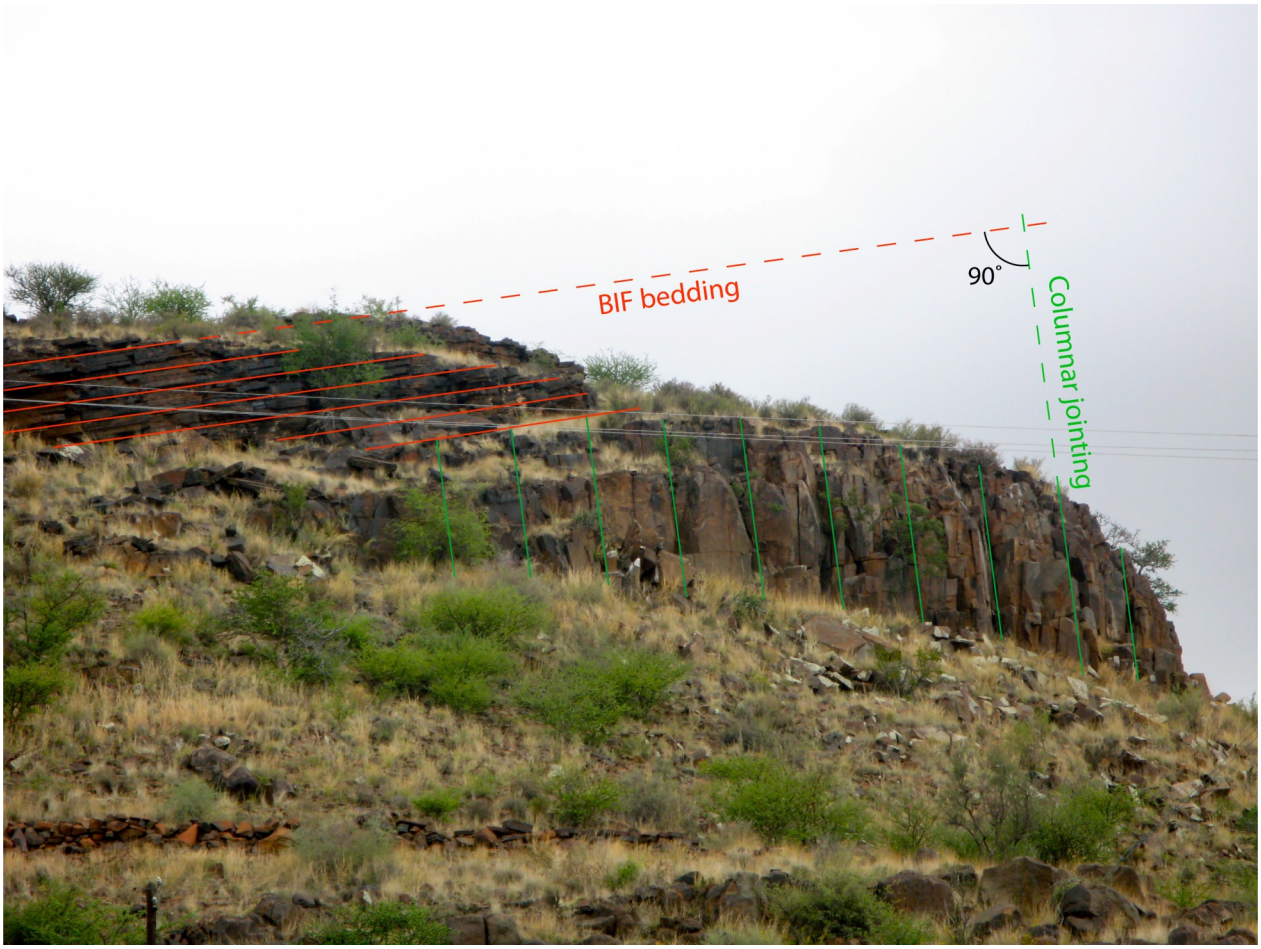

Fig. 3. Geological maps of the two study areas (see Fig. 2 for overview), including sites for paleomagnetic sampling. Simplified after Dreyer (1982).

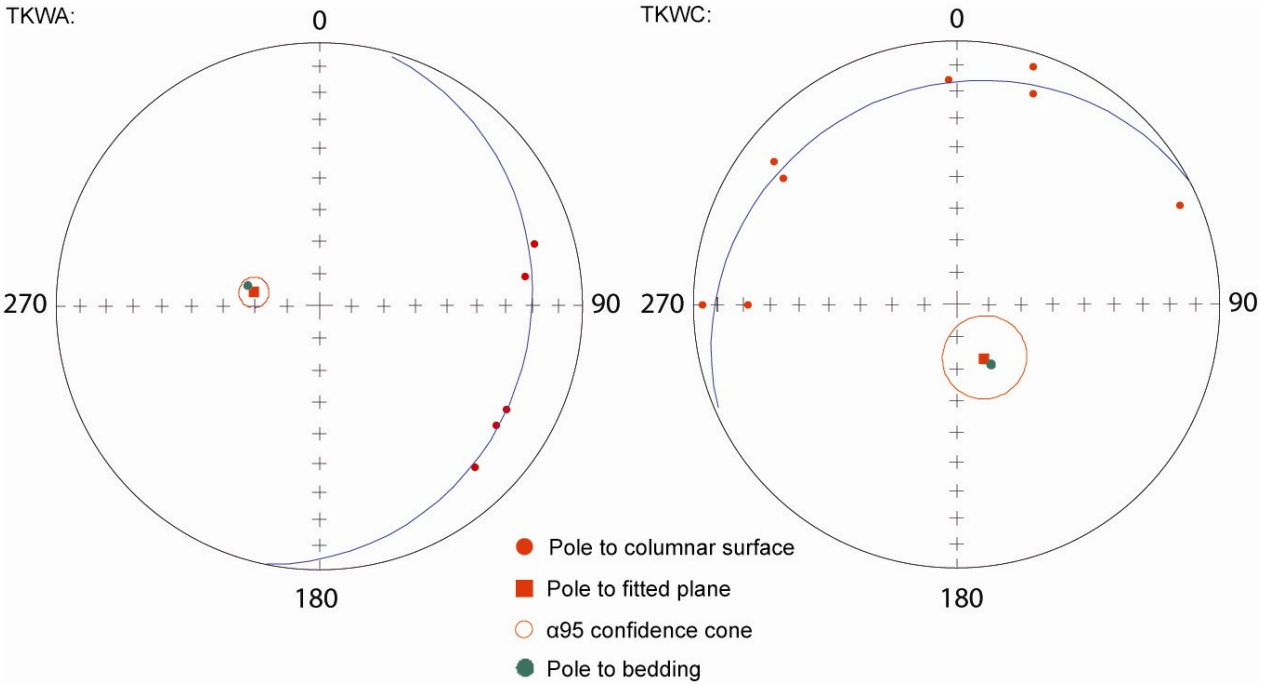

Fig. 9. Columnar jointing test used for classification of the Westerberg intrusion at locations TKWA and TKWC. The pole to the sedimentary bedding coincides within a 95% confidence cone with the sill emplacement direction. This direction is defined by the plane (great circle) that is formed by the poles of the columnar jointing surfaces. See Table 1 for bedding strike and dip values.

4 Methodology

4.1 TIMS Baddeleyite U-Pb Geochronology

The Westerberg dolerite (M03WA) was sampled for U -Pb geochronology by Michiel de Kock (University of Johannesburg). Sample processing and dissolution were performed at Lund University. Samples were crushed into cm-size pieces using a sledge hammer and then processed to a fine powder using a mill tray. Portions of approximately 30 g of suspended powder were transferred onto a Wilfley table. Baddeleyite grains are typically concentrated in the last mineral trace visible on the table. This final fraction was rinsed using a squirt bottle and collected in a large beaker. The heavy mineral aggregate was transferred to a petri dish and a pencil magnet was used to remove the magnetic minerals. Baddeleyite grains were hand-picked and separated from the remaining mineral phases (mostly apatite and pyrite) using a pair of tweezers under an optical microscope and then transferred to another petri dish using a handmade pipette. Further details are given by Söderlund and Johansson (2002).

In the clean laboratory, ethanol was added to the petri dish and the highest quality baddeleyite grains were identified visually. These grains were divided into 5 fractions comprising 3 - 4 grains each. The fractions were transferred into Teflon dissolution capsules and the grains were washed repeatedly in MQ -H_2O to dilute blank Pb in the ethanol and on crystal surfaces. After several rinses the grains were washed in ca. 3 N HNO_3 on a hot plate, followed by several rinsing steps in MQ-H_2O. After removal of all liquid, ca. 10 mg of tracer solution ($^{233-236}$U-^{205}Pb) was added to each capsule. 10 drops of HF and 1 drop of HNO_3 were applied to the baddeleyite grains. They were completely dissolved after three days in the oven at a temperature of 190°C.

The liquid phase was completely evaporated on a hot plate (100°C, ca. 2 hours). The sample was redissolved in 10 drops of 6.2 N HCl and one drop H_3PO_4 to convert fluorides to chlorides, and then dried on a hot plate. The sample was dissolved in 2 µl Si-Gel and then transferred to an outgassed Rhenium (Re)-filament. The sample was dried by applying an increasing current (from 1 to 2.3 A) until all phosphorous was burnt off.

Mass spectrometry analysis was performed using a Finnigan Triton Thermal Mass Spectrometer at the Swedish Museum of National History in Stockholm. The mass spectrometer is equipped with a Secondary Electron Multiplier (SEM) and RPQ-filter. Regression was carried out using the Isoplot macro by Ludwig (2003) with Uranium decay constants according to Jaffey et al. (1971). Initial common Pb correction was done using the isotopic compositions according to the global common Pb evolution model by Stacey and Kramers (1975).

4.2 Paleomagnetism sampling and laboratory processing

All drill sites for paleomagnetic studies (TKWA to E) were sampled by Tobias Kampmann (Lund University) and Michiel De Kock (University of Johannesburg). Cutting of specimens and further processing were performed in the paleomagnetic laboratory at the University of Johannesburg.

Seven to ten samples were drilled and extracted at each of the five sites along the banks of the Orange River. Three of the sites (TKWA, TKWB and TKWE) are located in the vicinity of the abandoned asbestos mining village of Westerberg, while the remaining sites are located to the east of Westerberg on the Naauwte farm. Further information on sampling sites is given in Table 1 and Fig. 3. Cores of 5 to 10 cm in length and 2.5 cm in diameter were drilled using a portable petrol-powered drill and extracted with hammer and chisel. For all cores, geographic orientation, hade and azimuth was measured with an orientation sleeve equipped with both a magnetic and a sun compass. Bedding strike and dip values are based on the bedding of the host BIF units and pole-plane calculations of the columnar jointing of the sill (Fig. 8).

Broken samples were glued with cement mixed from diatomaceous earth and sodiumsilicate solution in a room shielded from external magnetic influences. The samples were cut into specimens of 1.2 cm length and labelled with a white correction pen. This labelling survives high-temperature processing. All measure-

Table 1. Information on sampling sites

Site	Locality (°S,°E)	N	Lithology	Bedding (strike/dip)
Westerberg/Koegas				
TKWA	29.34°, 022.31°	10	Gabbro	11.6°/20.7°
TKWB	29.33°, 022.32°	7	Dolerite	14°/22°
TKWE	29.32°, 22.32°	10	Gabbro	344°/14° (1-6), 298°/28° (7-8)
Naauwte				
TKWC	29.45°, 022.62°	7	Gabbro	62.1°/18.6°
TKWD	29.45, 022.62°	8	Dolerite	62.1°/18.6°

ments of magnetic remanence were made by using the superconducting rock magnetometer at the University of Johannesburg (vertical 2G Enterprises DC-4K with 3 axes SQuID sensors). Specimens were exposed to stepwise demagnetization including an alternating-field (AF) pre-treatment with a high-field degausser which is inline with the magnetometer. Steps included 0, 2, 4, 6 and 8 kA/m. This was followed by thermal demagnetization using an ASC Model TD48 shielded oven at temperature steps of 100, 200, 250, 350, 425, 475, 500, 515, 530, 540, 545 and 550 °C. The process was abandoned when samples started to show unstable behaviour due to their magnetization dropping below that of the sample handler of the magnetometer.

Identification and fitting of magnetic components were made by least-squares component analysis (Kirschvink, 1980) using the software Paleomag 3.1b2 (Jones, 2002). Linear fits were included in subsequent analyses if they had a mean angle deviation (MAD) equal to or less than 10°. Additional digital handling was conducted with the PmagPy software (Tauxe et al., 2010). Paleomagnetic pole calculation is based on the assumption of a geocentric axial-dipole field and a stable earth radius throughout geological time that equals the present day radius. Paleogeographic reconstructions based on the poles obtained were performed with the software PaleoMac (Cogné, 2003).

5 Results

5.1 Baddeleyite morphology

The sample taken for U-Pb dating (sample M03WA) is from the centre of the Westerberg sill in the Westerberg area (paleomagnetism site TKWA). Extracted baddeleyite grains are 30 to 50 µm in length, elongated and brownish in colour with 'frosty' surfaces when viewed under an optical microscope. The latter property is indicative of replacement of baddeleyite by zircon ($ZrSiO_4$) as a result of a postmagmatic reaction with silica-rich fluid. As baddeleyite is fragile, the crystals of the sample might often be anhedral fragments of originally larger grains. Fig. 10 comprises scanning electron microscopy (VP-SEM) images of representative baddeleyite grains with unpolished grains above and polished grains below (ca. 30 minutes using a 1 µm diamond polishing pad). The SEM images reveal a scattered distribution of zircon recognizable as light spots preferentially at or close to the rims. SEM-EDS analyses of unpolished grains also indicate the presence of thin and minor Fe-(Ni-Cr) sulphides, probably of secondary origin. One grain has remnants of pyroxene attached to its surface (Fig. 10a). In polished sections, zircon is restricted to ca. 0.5 µm thick semi-continuous rims around the grains. Zir

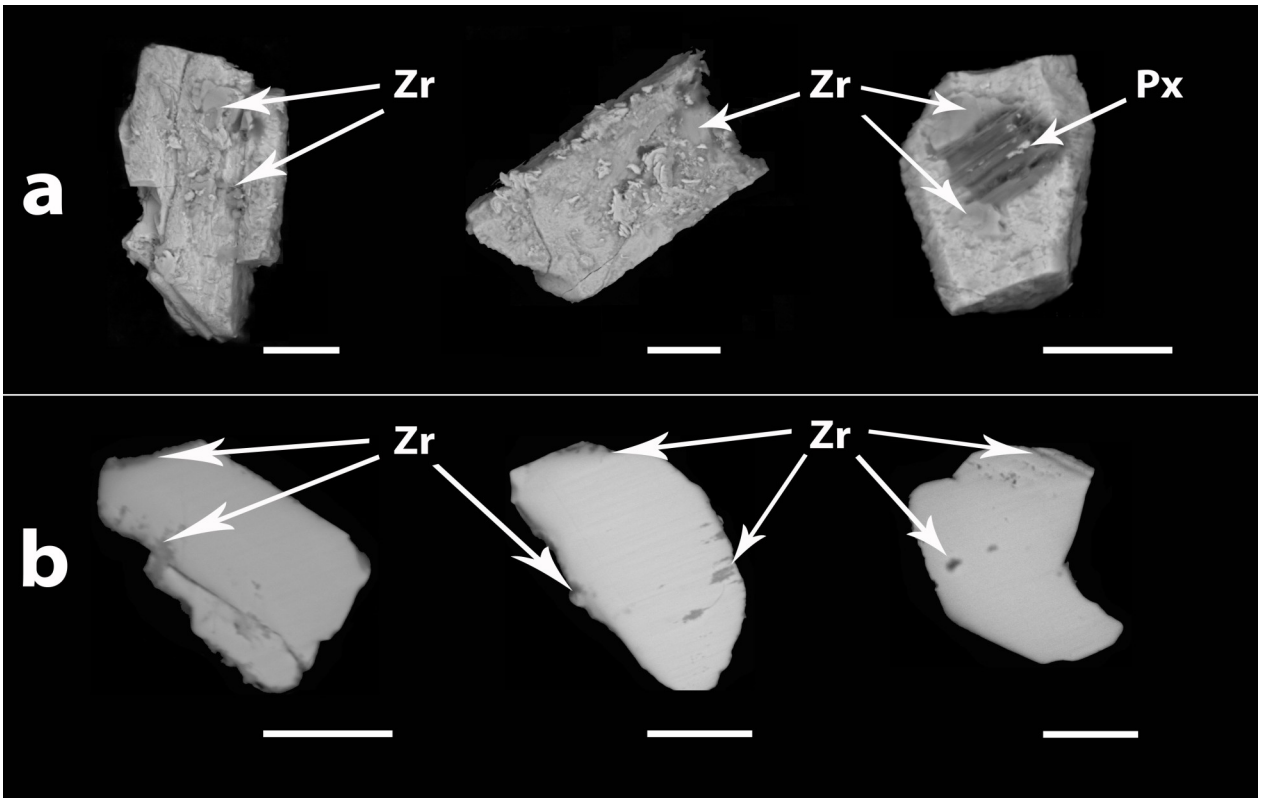

Fig. 10. SEM-BSE images of (a) baddeleyite grain surfaces and (b) polished cross-sections. Surface images show zircon domains on the grains and images of polished grains reveal thin zircon alteration along parts of the rims. White arrows point out zircon domains (Zr) and one adjoining pyroxene crystal (Px). Due to lower density, zircon shows up darker in backscattered electron analysis (BSE). The white scale bar for each grain represents a length of 10 µm.

con is also present in fractures, indicating an influx of silica-rich fluid after crystallisation of baddeleyite (Fig. 10b).

5.2 U-Pb geochronology

60 baddeleyite grains were extracted from sample M03WA of the Westerberg intrusion. Five fractions of three to four grains each were analysed. Table 2 shows the obtained TIMS U-Pb data. The $^{207}Pb/^{206}Pb$ ages range from 2405.8 ± 1.6 to 2420.2 ± 1.7 Ma. The fractions show 2 to 4% discordant plots on a Concordia diagram and comparably low $^{204}Pb/Pb_{total}$ ratios (1 to 4%). Since Pb is highly incompatible in baddeleyite (and zircon), almost all Pb in the sample must have derived from the radioactive decay of uranium.

A free regression of all five fractions produces an upper intercept age of 2437.1 ± 5.9 Ma and a lower intercept age of 898 ± 140 Ma (MSWD = 2.0). For various reasons given below, a forced lower intercept of 1010 ± 100 Ma is preferred for calculating the regression. This results in a slightly older age of 2442.1 ± 5.1 Ma (MSWD = 2.1), which is here considered the best estimate for the age of the Westerberg sill. Both free and forced Concordia diagram regressions are shown in Fig. 11.

5.3 Paleomagnetism

5.3.1 Description of demagnetization behaviour

The Westerberg sill samples show three distinguishable demagnetization profiles (Fig. 12). Samples from site TKWA (Fig. 12a) are characterised by a steep drop in magnetization during AF pre-treatment and low-temperature demagnetization steps, as well as a sudden transition into a shallow plateau at very low levels of magnetization (< 1 mAm^2). A small hump at TT 200°C to TT 250°C indicates a shift into the medium-temperature carrier phase. Usually samples begin to behave unstably at around TT 475°C. Samples from sites TKWB and TKWE (Fig. 12b) typically show a stable plateau in the low to medium temperature range and a gradual transition into the characteristic components when reaching TT 475°C. Samples begin to behave unstably above ca. TT 530°C, but can also show stable behaviour up to TT 550°C. Fig. 12c is a representative demagnetization profile for sites TKWC and TKWD. Three peaks of loss of magnetization can be recognized; during AF pre-treatment, in the TT 200°C to TT 350°C and above TT 475°C. The three humps are separated from one another by stable plateaus and represent transitions between the distinct mineral phases that act as magnetization carriers.

Stepwise demagnetization of the paleomagnet-

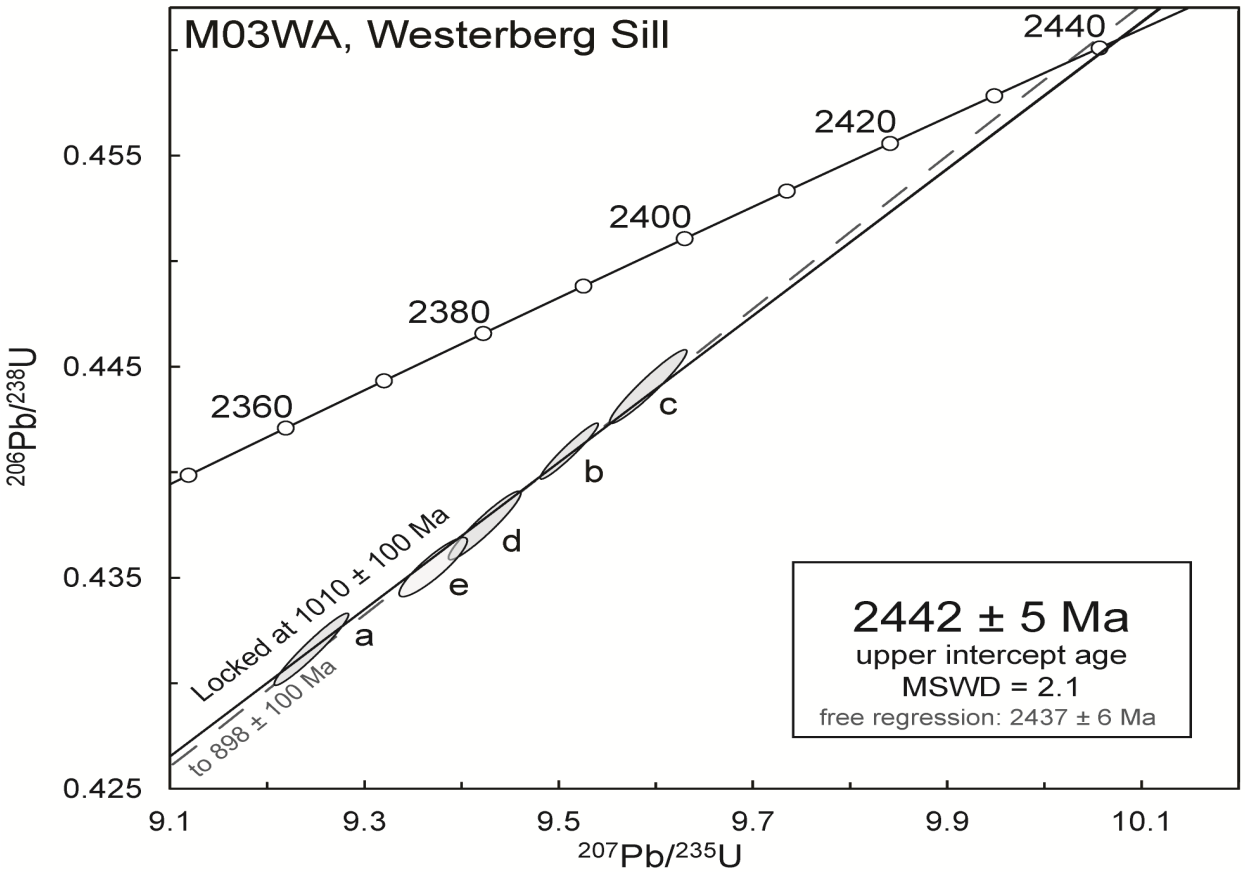

Fig. 11. Concordia diagram plots of an unforced (dashed line) and forced (solid line) lower intercept for the regression using a lower intercept at 1010 ± 100 Ma in the latter.

Table 2. U-Pb TIMS data

Analysis no. (number of grains)	U/ Th	Pbc/ Pbtot[1)]	$^{206}Pb/^{204}Pb$ raw[2)]	$^{207}Pb/^{235}U$ [corr][3)]	± 2s % err	$^{206}Pb/^{238}U$	± 2s % err	$^{207}Pb/^{235}U$ [age, Ma]	$^{206}Pb/^{238}U$	$^{207}Pb/^{206}Pb$	± 2s % err	Concord-ance
A (3 grains)	21.1	0.013	4623.5	9.2468	0.34	0.43166	0.32	2362.8	2313.2	2405.8	1.6	0.962
B (3 grains)	35.0	0.007	9006.7	9.5125	0.26	0.44104	0.25	2388.8	2355.3	2417.4	1.2	0.974
C (3 grains)	54.5	0.015	3955.1	9.5940	0.34	0.44409	0.32	2396.6	2368.9	2420.2	1.7	0.979
D (4 grains)	30.2	0.030	1892.0	9.4254	0.32	0.43752	0.30	2380.3	2339.5	2415.4	1.8	0.969
E (4 grains)	26.5	0.041	1320.1	9.3723	0.31	0.43555	0.26	2375.1	2330.7	2413.5	2.4	0.966

[1)] Pbc = common Pb; Pbtot = total Pb (radiogenic + blank + initial).
[2)] measured ratio, corrected for fractionation and spike.
[3)] isotopic ratios corrected for fractionation (0.1% per amu for Pb), spike contribution, blank (0.6 pg Pb and <0.1 pg U), and initial common Pb. Initial common Pb corrected with isotopic compositions from the model of Stacey and Kramers (1975) at the age of the sample.

Table 3. Fisher-statistical revision of the least-squares component analysis after Kirschvink (1980).

Component A			Geographic				Tilt-corrected			
Area	**Site**	**n/N**	**Decl**	**Incl**	**κ**	**α95**	**Decl**	**Incl**	**κ**	**α95**
Westerberg	TKWA	10/10	195.6	-76.6	1.58	53.2	4.2	-83	1.58	53.2
	TKWB	7/7	136	0.9	1.21	87.2	134	-11	1.21	87.22
	TKWE	8/8	299.8	24.1	4.49	26.5	301.4	31.4	3.72	29.82
Naauwte	TKWC	10/10	336.8	41	1.07	102	349.6	37.1	1.07	101.7
	TKWD	7/7	44.2	-36.7	45.5	8.36	55.4	-49	45.3	8.38
Component B			Geographic				Tilt-corrected			
Area		**n/N**	**Decl**	**Incl**	**κ**	**α95**	**Decl**	**Incl**	**κ**	**α95**
Westerberg		12/25	32.6	-52.1	17	16.7	52	-66	17	16.71
Naauwte		8/17	28.2	-43.3	22.5	9.84	12.4	-52	18.1	11.04
Component C			Geographic				Tilt-corrected			
Area		**n/N**	**Decl**	**Incl**	**κ**	**α95**	**Decl**	**Incl**	**κ**	**α95**
Naauwte (TKWC1-5)		5/25 (5/10)	166	79.6	5.08	32.9	92.7	71	5.09	32.9
Component D			Geographic				Tilt-corrected			
Area		**n/N**	**Decl**	**Incl**	**κ**	**α95**	**Decl**	**Incl**	**κ**	**α95**
Westerberg		10/25	87.8	-72.5	10.3	15.8	328.6	-85	9.2	15.37
Naauwte		17/17	188	-70.3	5.2	26.8	194.5	-52	3.7	31.44
Component E			Geographic				Tilt-corrected			
Area		**n/N**	**Decl**	**Incl**	**κ**	**α95**	**Decl**	**Incl**	**κ**	**α95**
Westerberg (TKWA9)		1/25 (1/10)	22.7	-55.5	-	-	18.9	-35	-	-
Naauwte (TKWD)		7/17 (7/7)	31.4	-12.5	63.2	8.04	33.1	-28	63.4	8.03

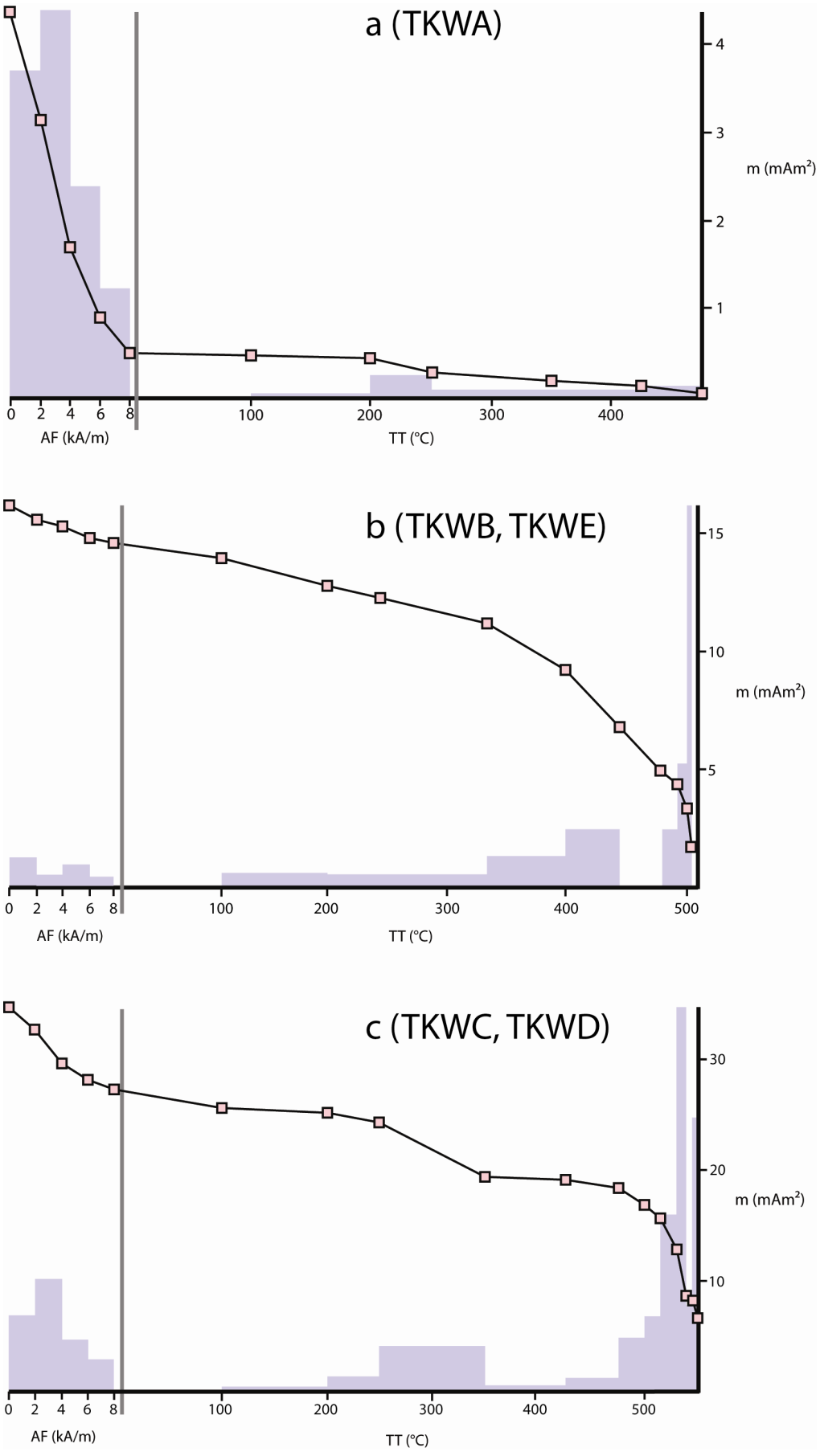

Fig. 12. Three representative J/J_0 demagnetization profiles of a Westerberg sill specimen.

TKWA5:

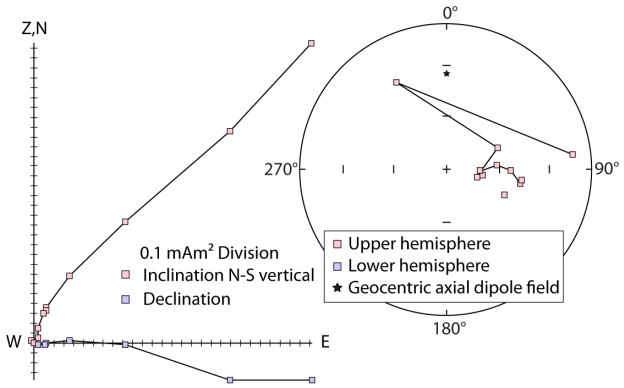

TKWA9:

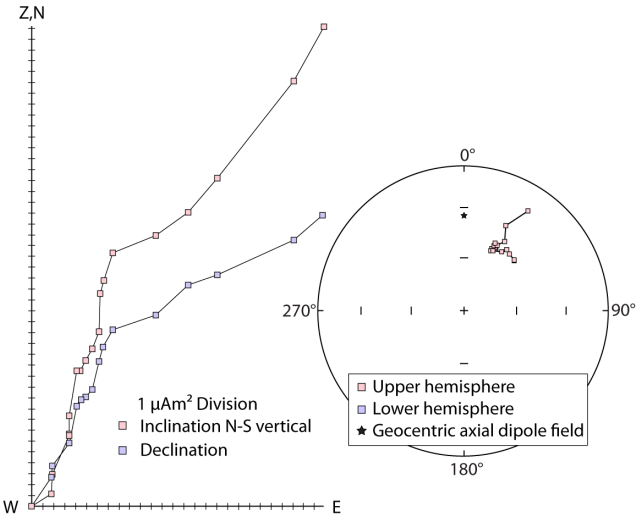

TKWB4:

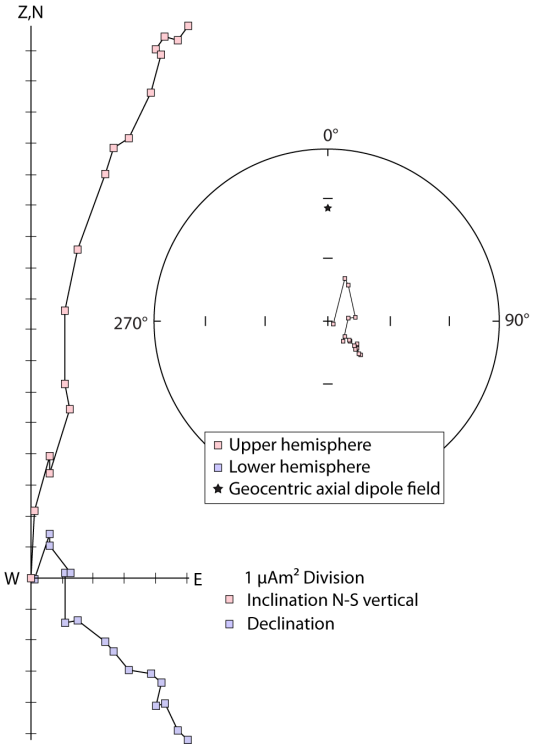

TKWB5:

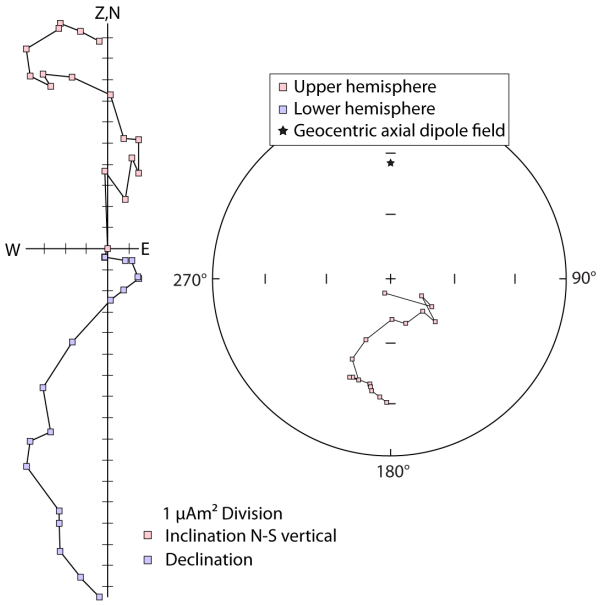

TKWC1:

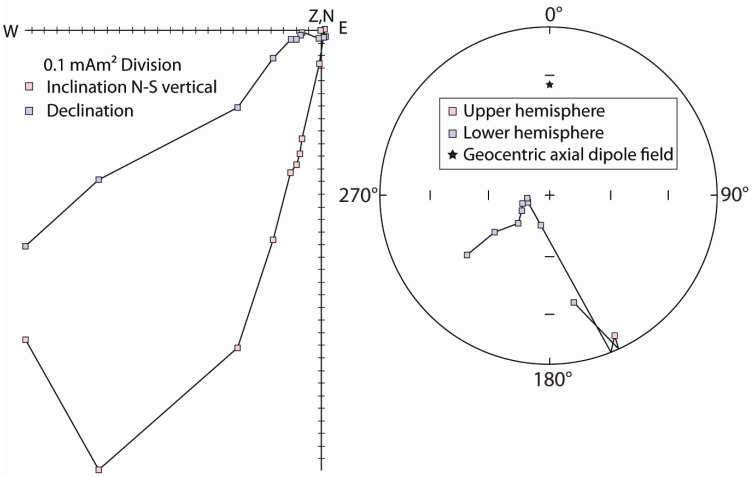

TKWC5:

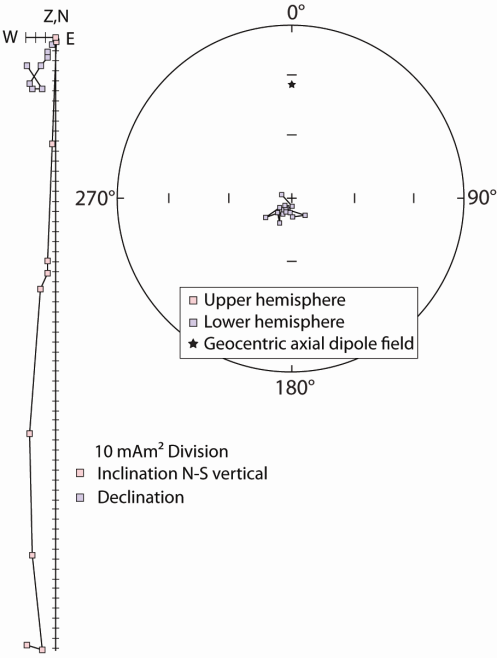

TKWC9:

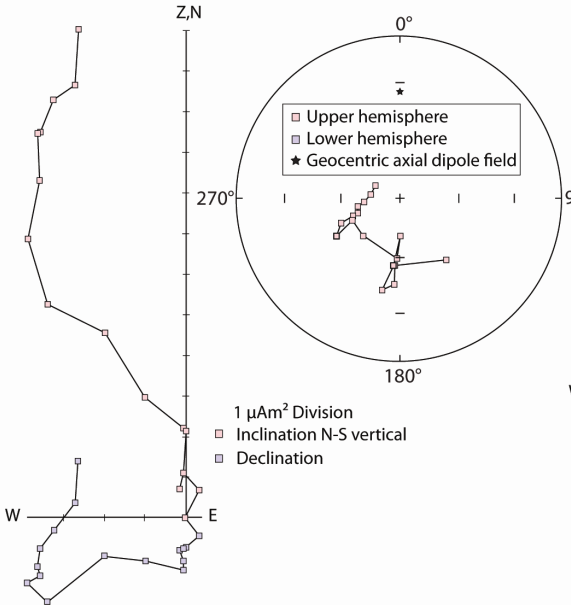

TKWC10:

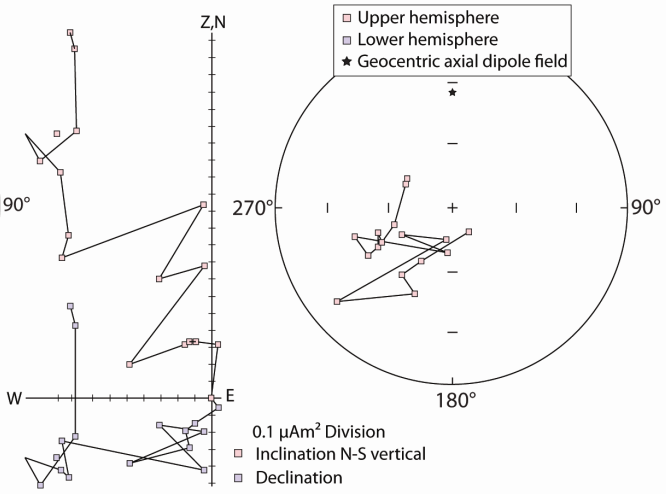

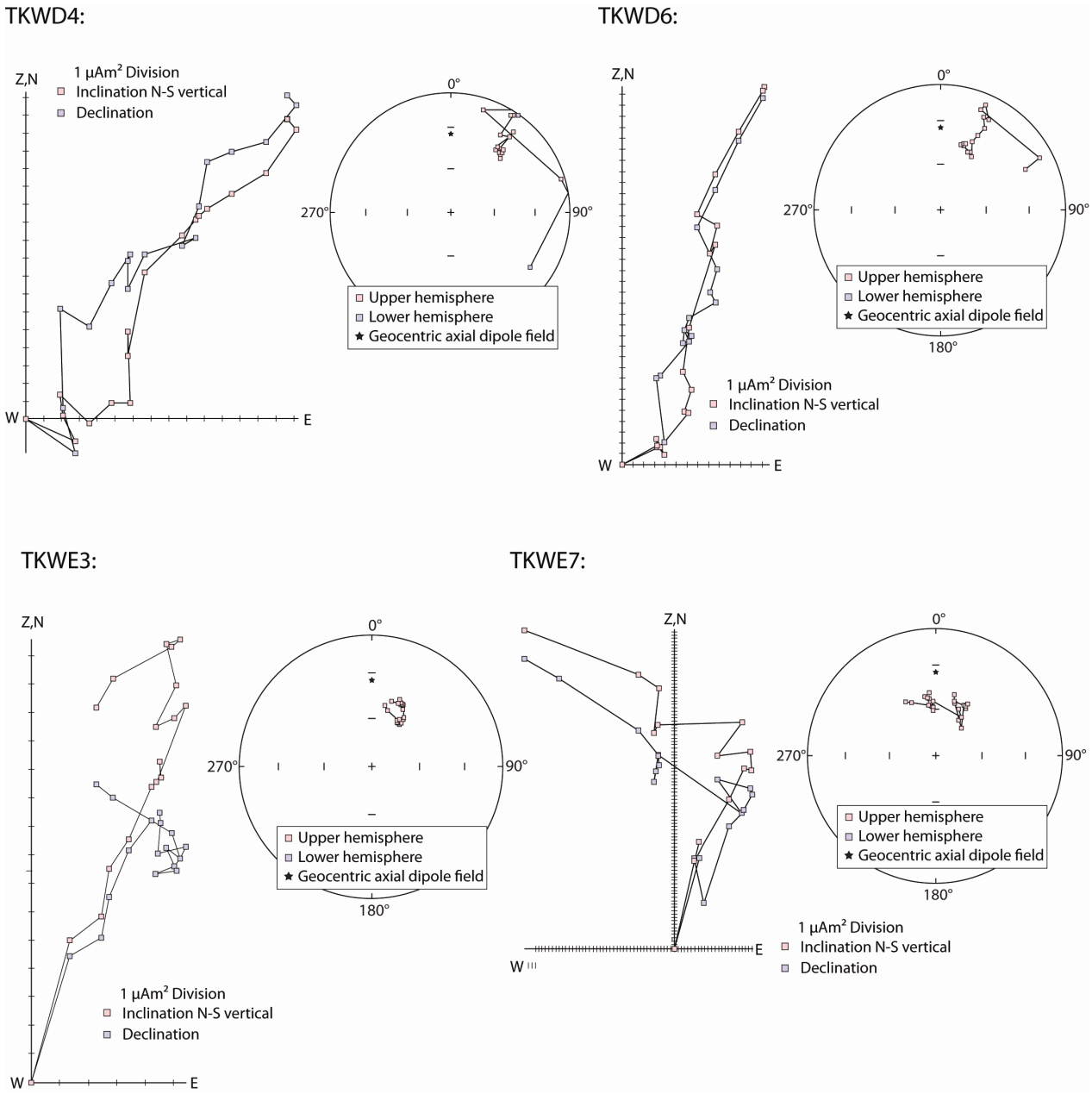

Fig. 13. Orthographic and equal-area stereonet illustrations of demagnetization behaviour of selected samples from the five investigated sites. Samples TKWC9 and TKWC10 represent a felsic dykelet intruding the Westerberg sill (Fig. 18).

5.3.2 Component A (AF, low stability)

A low stability and low coercivity component (here referred to as Component A), common to all sites, was usually removed after either AF pre-treatment or the first temperature demagnetization step (TT 100°C). The vectors of the remanent magnetization are mostly randomly oriented. They may represent isothermal remanent magnetization in response to lightning strikes or low stability magnetization due to the sampling and/or the preparation process. An exception is samples from site TKWD. These samples tend to display north-westerly and upward pointing vectors during AF pre-treatment and low levels of thermal demagnetization. A high degree of scatter between individual samples from site TKWD hampers statistical quantification (Table 3 and Fig. 14). However, the direction is very similar to the predominant Component B direction (Fig. 15).

5.3.3 Component B (TT 100°C to TT 550°C)

After the removal of Component A, the samples display variable behaviour reflecting the range of grain size samples. The majority of samples (all samples from sites TKWE and TKWD, two samples each from both site TKWB and site TKWA and one sample from site TKWC) display a north-easterly and upward directed component (here referred to as Component B) with moderate inclination after the removal of Component A. Removal of Component B generally took place in the temperature range of TT 100°C to TT 550°C. Samples from site TKWE are dominated by Compo-

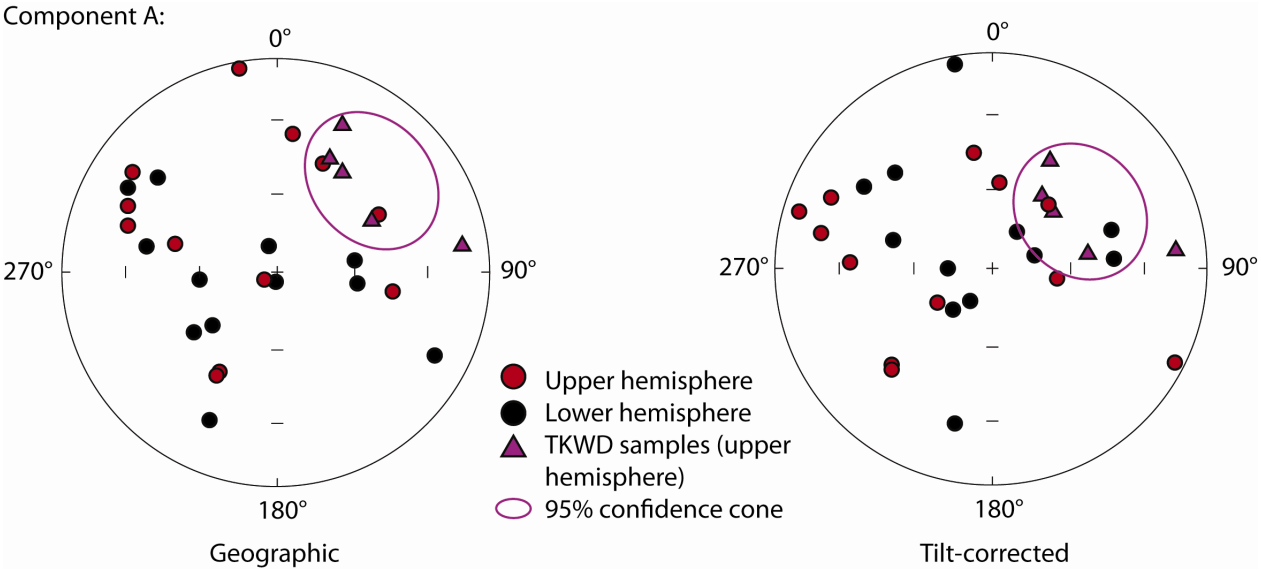

Fig. 14. Distribution of Component A (low stability) from all sites is random, except for samples from site TKWD. Here, low stability vectors (triangles) form a weak grouping in a north-easterly and upward direction. The ellipses represent 95% cones of confidence around the mean calculated from all low stability components at site TKWD.

nent B at high temperature steps (between TT 474°C to TT 550°C). Here, Component B is the characteristic magnetization (i.e. demagnetization vectors are directed towards the origin). At site TKWD, demagnetization vectors of Component B are not directed towards the origin. Another more stable component is still present. Only two samples from site TKWA display Component B. These are TKWA9 and TKWA10. These two samples originated from a roadcut high above the Orange River and far removed from the rest of the samples of this site. These two samples were also spatially closer to the margin of the sill and therefore much finer grained than the rest of TKWA samples. Two samples from site TKWB also display Component B. These are samples TKWB6 and TKWB7. There is no obvious reason why other samples from site TKWB did not record Component B. One probable cause may be an as yet unidentified grain size control on the magnetic moment that is recorded.

Results of samples from sites TKWA, TKWB and TKWE were combined to calculate a component mean for the Westerberg area, while samples from site TKWD were used to calculate a component mean for the Naauwte area (Table 3). Without applying a structural correction to restore beds to paleohorizontal, the Component B means for the Naauwte and Wester-

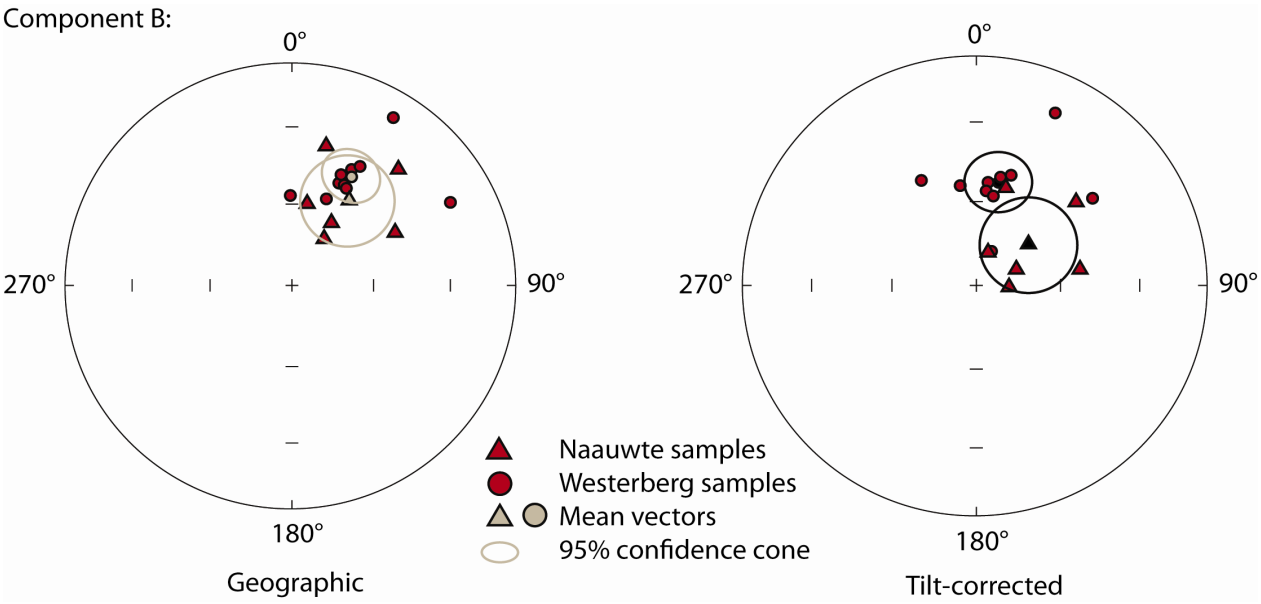

Fig. 15. Distribution of Component B from all sites in the Westerberg area (TKWE, TKWB, TKWA = circles) and in the Naauwte area (TKWC = triangles). Samples from site TKWD are not included. A clear worsening in the grouping of data is observed upon application of a structural correction to restore beds to paleohorizontal. The ellipses represent the 95% cones of confidence around the calculated means.

berg areas are indistinguishable from one another. If beds are unfolded, the components obtained from opposite limbs of a synclinal structure differ significantly from one another (Fig. 15). This suggests strongly that the Component B was acquired after folding took place.

An average mean for Component B can thus be calculated by combining the measurements (not corrected for tilt) of 17 samples from the Westerberg and Naauwte sites (Decl. = 29.6°, incl. = -46.4°, α95 = 8.11°, κ = 20.31).

5.3.4 Component C (TT 100°C to TT 425°C)

After the removal of Component A, samples TKWC1 to TKWC5 from the Naauwte area do not display Component B. Instead, they display a south-westerly downward directed component that does not point towards the origin. This component (here referred to as Component C) is revealed in a temperature range from TT 100°C to TT 425°C. An average mean for Component C can be calculated by combining these five samples from the Naauwte area (Geographic decl. = 207.6°, incl. = 61.6°, α95 = 25.83°, κ = 9.73; Stratigraphic decl. = 168.4, incl. =73.4, α95 = 26.05°, κ = 9.58). Component C unblocks in a similar temperature range as Component B and is about 180 degrees removed from Component B (Fig. 16).

5.3.5 Component D (TT 200°C/500°C to TT 550°C)

A fourth component (here referred to as Component D) is removed in a variable temperature range from TT 200°C to TT 550°C (in some cases TT 500°C to TT 550°C as characteristic components), generally in samples from sites TKWB, TKWC and TKWD. A few samples from other sites (TKWA4, TKWA5 and TKWE2) also display groupings recognizable as Component D. These vectors are somewhat scattered, but all directed steeply upwards. Most samples point south-easterly. Samples from sites TKWA, TKWB and TKWE can be combined to calculate a component mean for the Westerberg area, while samples from site TKWD can be used to calculate a component mean for the Naauwte area (Table 3). Without applying a structural correction to restore beds to paleohorizontal, the Component D means at Naauwte and Westerberg are fairly similar to one another. If the syncline is unfolded, the vectors obtained from opposite limbs diverge. This suggests strongly that Component D was acquired after folding occurred. The component is also recorded as a characteristic, high-temperature component in samples TKWC9 and TKWC10. These were taken from a felsic dykelet, with a thickness of ca. 5 cm, intruding the Westerberg sill (Fig. 18). This allows for the interpretation that Component D represents viscous remanent magnetization related to a younger magmatic event. The dykelet has the same north-south orientation generally (strike 221°), as do numerous dykes in the area (Fig. 3). This event is recorded in the majority of sites and, therefore, could well be of a regional scale.

A combined mean can be calculated from Component D in the Naauwte and Westerberg areas (Geographic decl. = 131.1°, incl. = -77.9°, α95 = 14.95°, κ = 6.32).

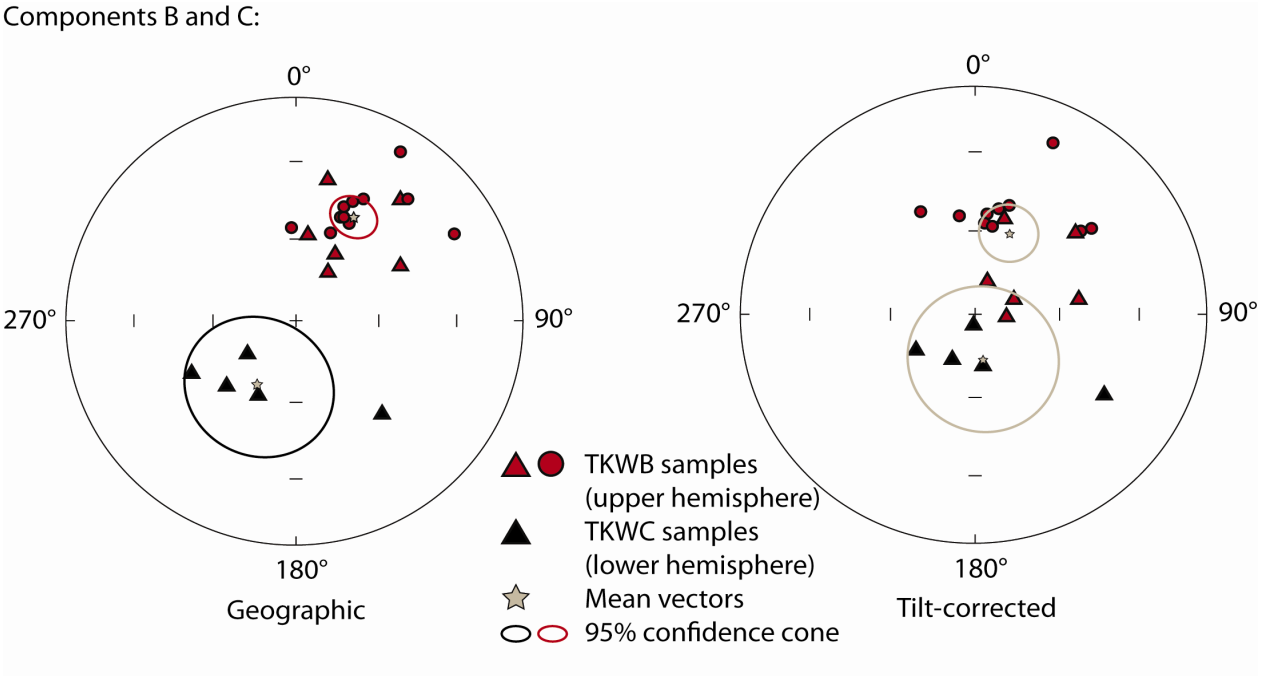

Fig. 16. Distribution of Component C from all sites in the Naauwte area (TKWC1 to TKWC5 = triangles), and Component B for comparison (Fig. 15). Components B and C are nearly 180° apart and recorded in a dual polarity overprint. Therefore, they are probably related to one another.

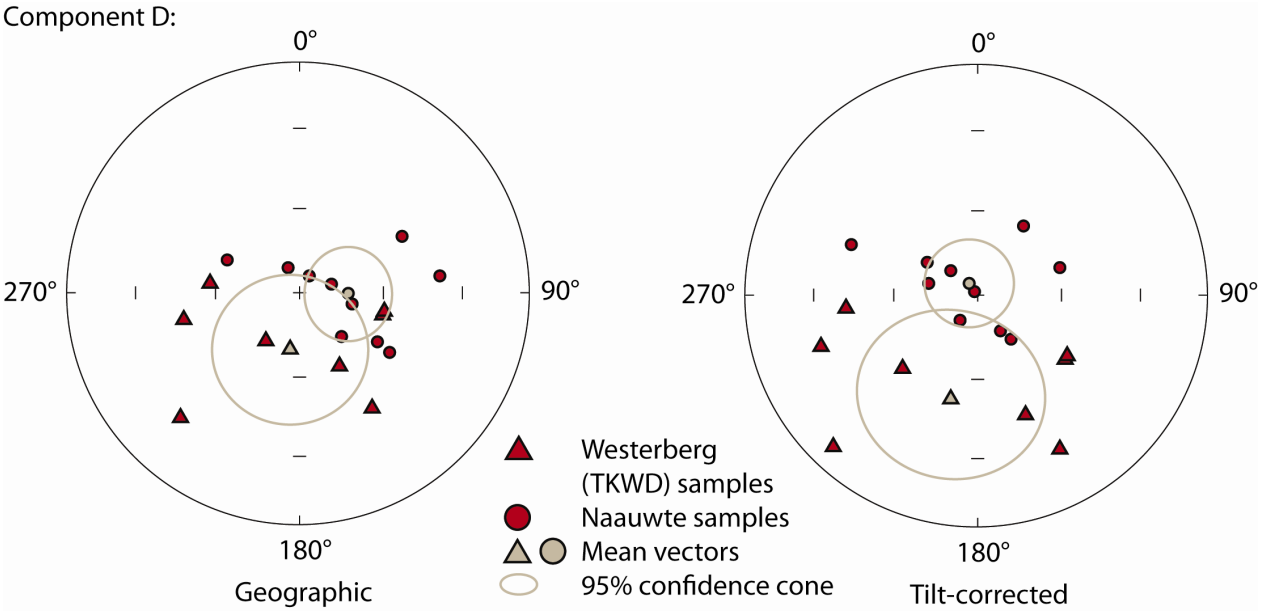

Fig. 17. Distribution of Component D in the Westerberg area (TKWB, TKWA4 to 5 and TKWE2 = circles) and from Naauwte (TKWC, TKWD = triangles).

Fig. 18. Felsic dykelet of ca. 5 cm thickness intruding the Westerberg sill at site TKWC (paleomagnetism samples TKWC9 and TWC10).

5.3.6 Component E (TT 500°C to TT 550°C)

After the removal of Component D, characteristic components (here referred to as Component E) unblock in samples from site TKWD and one sample from site TKWA. Demagnetization pattern moves away from Component D towards a northerly and shallow direction in the temperature range TT 500°C to TT 550°C. Component E is revealed in only eight out of a total of 42 samples (i.e. in about 20% of samples). Samples from TKWD and sample TKWA9, which recorded this Component E, are all from near the contact of the sill with the BIF and of similar grain size. Unfortunately, only one sample from the Westerberg area recorded Component E (TKWA9) compared to the seven samples from the Naauwte area (TKWD). This prevents an evaluation of relative timing of the acquisition of Component E. Given the orientation of the fold axis and relatively shallow dips of the respective limbs in the Westerberg and Naauwte areas, the outcomes of a fold test probably would not have been of much use. This is due to Component E (Fig. 19) being nearly parallel to the fold axis in the area (Fig. 4), so unfolding would not result in a significant change in grouping. Of all the components revealed, I favour this characteristic direction as being the oldest. Component E is overprinted by post-folding components D and B, Component C is nearly antipodal and probably related to Component B. Component A represents random low-stability directions.

The combined mean for Component E is: Tilt-corrected decl. = 35.7°, incl. = -9.1°, $\alpha 95 = 10.65°$, $\kappa = 30.34$.

6 Discussion

6.1 Emplacement age of the Westerberg sill

The free regression yielding a 2437 ± 6 Ma upper intercept age results in a lower intercept age of 898 ± 150 Ma (Fig. 11). SEM analysis of baddeleyite shows 'frosty' surfaces (Fig. 10), being alteration rims of zircon around the baddeleyite grains. These observations suggest that the baddeleyite suffered a partial phase transition to zircon that can be linked to the Namaqua-Natal metamorphic event. The final regression line thus connects the two Pb/U end members of the original baddeleyite phase and the Pb-depleted zircon phase. Pb/U compositions of the grains plot along this line according to the degree of zircon replacement. Gnos et al. (2003) presented a norrishite ($KMn_2LiSi_4O_{12}$) ^{40}Ar-^{39}Ar age of 1011 ± 7 Ma from a manganese ore body at the Wessels Mine, close to Hotazel in the Northern Cape Province of South Africa, ca. 250 km north of the study area. The results obtained indicate that metamorphic activity continued until ca. 1.01 Ga. The final stages of orogenic events are commonly thought to be associated with increased fluid activity, which might have been responsible for the silica reaction observed. Therefore, the baddeleyite age regression is forced through 1010 ± 100 Ma which results in an upper intercept age of 2442 ± 5 Ma, interpreted as the best estimate of the emplacement age of the Westerberg sill.

Another orogenic event (pre-1.93 Ga) is held responsible for the folding in the area (De Kock, 2007). Another earlier hydrothermal alteration effect

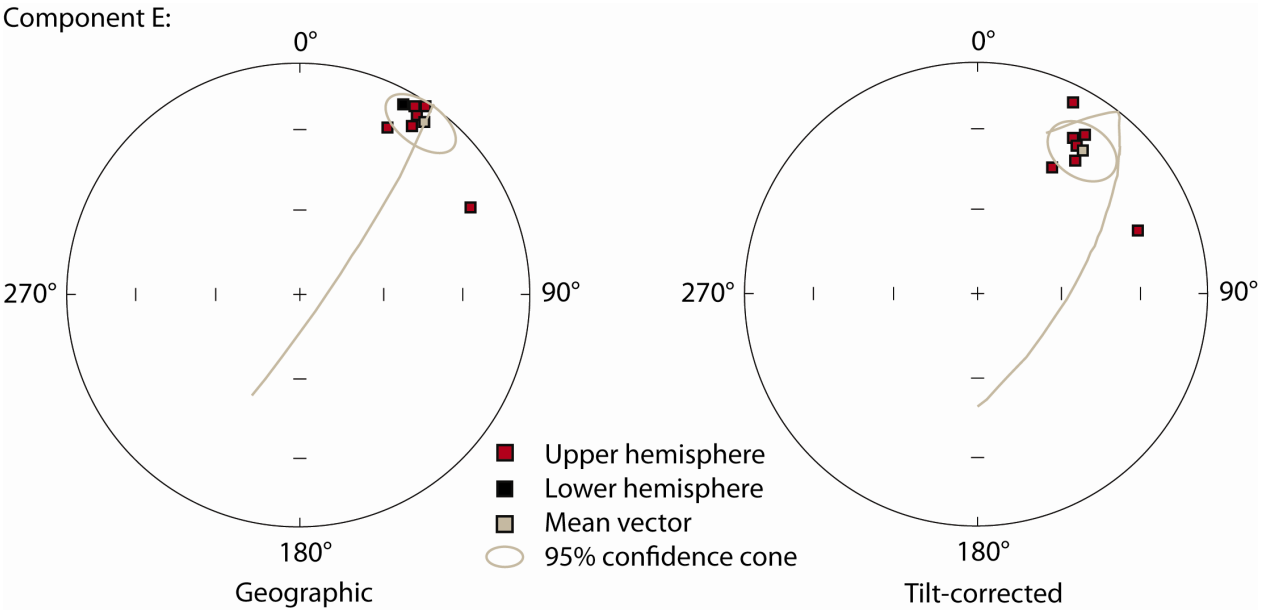

Fig. 19. Distribution of Component E in the Naauwte area (TKWD = squares).

on the baddeleyite grains related to this event is conceivable, but not observed in the SEM analysis of the grains. Polymetamorphic zircon growth would result in complex zircon rims and structures which are lacking in the baddeleyite grains of the Westerberg dolerite (Fig. 9). Furthermore, a multi-stage disturbance of the U-Pb isotopic system would result in both false lower and upper intercept ages (e.g. Söderlund, 1996). In this case, a single-grain zircon U-Pb age of ca. 2500 Ma for tuffite units at the base of the Kuruman BIF (Trendall et al., 1995) is thought to reflect the age of the onset of BIF sedimentation (Eriksson et al., 2006). Therefore, it also represents a maximum age of the Westerberg sill. Another zircon U-Pb age of 2465 ± 7 Ma (Martin et al., 1998) from the upper Kuruman Formation is probably a fair estimate of the transition to a somewhat shallower depositional environment, resulting in deposition of the overlying Daniëlskuil Formation (Eriksson et al., 2006). The age result of this study agrees with these previously obtained ages. Therefore, a polymetamorphic effect on the U-Pb system of the baddeleyite grains can also be ruled out.

Field observations and thermal alteration of the surrounding country rock support the assertion that the Kuruman BIF was already lithified when the intrusion occurred. Consequently, the age of 2442 ± 5 Ma for the Westerberg sill reflects a minimum age of this formation and might have coincided with the deposition of the 2432 ± 31 Ma Daniëlskuil Formation (SHRIMP U-Pb zircon age, obtained by Trendall et al., 1990).

6.2 Paleomagnetism

6.2.1 Characterization of secondary components

Based upon the worsening of the grouping of Component B amongst the various sites once beds are restored to horizontal, it can be concluded that this component is secondary and postdates the regional folding. A virtual geomagnetic pole (VGP) can be calculated at 64.0° N, 116.0° E, dp = 6.7° and dm = 10.4°. The pole for the near antipodal Component C (64.2° N, 151.2° E, dp = 31.0° and dm = 40.2°) is statistically indistinguishable from the VGP for Component B. It is suggested that these two components represent a dual polarity overprint recorded in the Westerberg sill. Although Component B is in the proximity of the time averaged dipole field of South Africa (northerly and steeply upward directed), it is consistently northeast thereof and less steep than expected. It bears even less similarity to the present geomagnetic field at the sampling sites. Together with the presence of component C, this implies an older age. The component does not show any resemblance to Jurassic and Cretaceous poles from South Africa, both periods of extensive basaltic magmatism and kimberlite intrusion respectively. The calculated poles are also very different from poles reported from the ca. 1.01 Ga Namaqua-Natal Metamorphic Province immediately to the west of the sampling area. The closest match with published poles is with Paleogene and Neogene poles from Africa (Fig. 20). It can be speculated that this dual polarity overprint is the result of weathering associated with the uplift of southern Africa during the Early Miocene to create the Post-African land surface (Partridge et al., 2006).

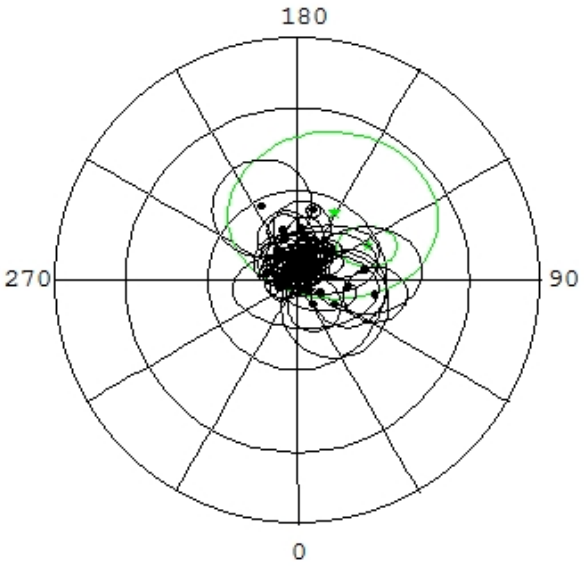

Fig. 20. Comparison of VGPs calculated for components B and C (green stars) and Paleogene and Neogene poles from the African continent (black dots). Paleopoles are taken from the Global Paleomagnetic Database (Pisarevsky, 2005).

Component D also displays a worsening of groupings when bedding is restored to paleohorizontal. Once more this suggests that the component was acquired after regional folding. A VGP can be calculated at 13.0° N, 184.8° E, dp = 26.4° and dm = 28.1°. The relatively poor grouping of data might be due to mixing of two discrete magnetic components, but they could not be identified. However, compared with known poles from the Kaapvaal Craton, a similarity with poles from the ca. 1.01 Ga Namaqua-Natal Metamorphic Province immediately to the west of the sampling area is noticeable (Fig. 21). These pole directions are also similar to the pole from the 1.93 Ga Hartley lava which provides the maximum age for the Kheis orogeny (Cornell et al., 1998). Regional folding predates both the Kheis and the Namaqua-Natal orogenies, but these two events might have refolded the region during its complex history. Component D is interpreted as being related to either the Namaqua-Natal or to the older Kheis orogeny. Lower intercept ages for baddeleyite grains close to the age of the Namaqua-Natal orogeny (this study) favour Component D being a 1.01 Ga overprint. The metamorphic overprint on western cratonic units, affected by the Namaqua-Natal orogenic event, does not exceed lower greenschist facies (Crow and Condie, 1988). Miyano and Beukes

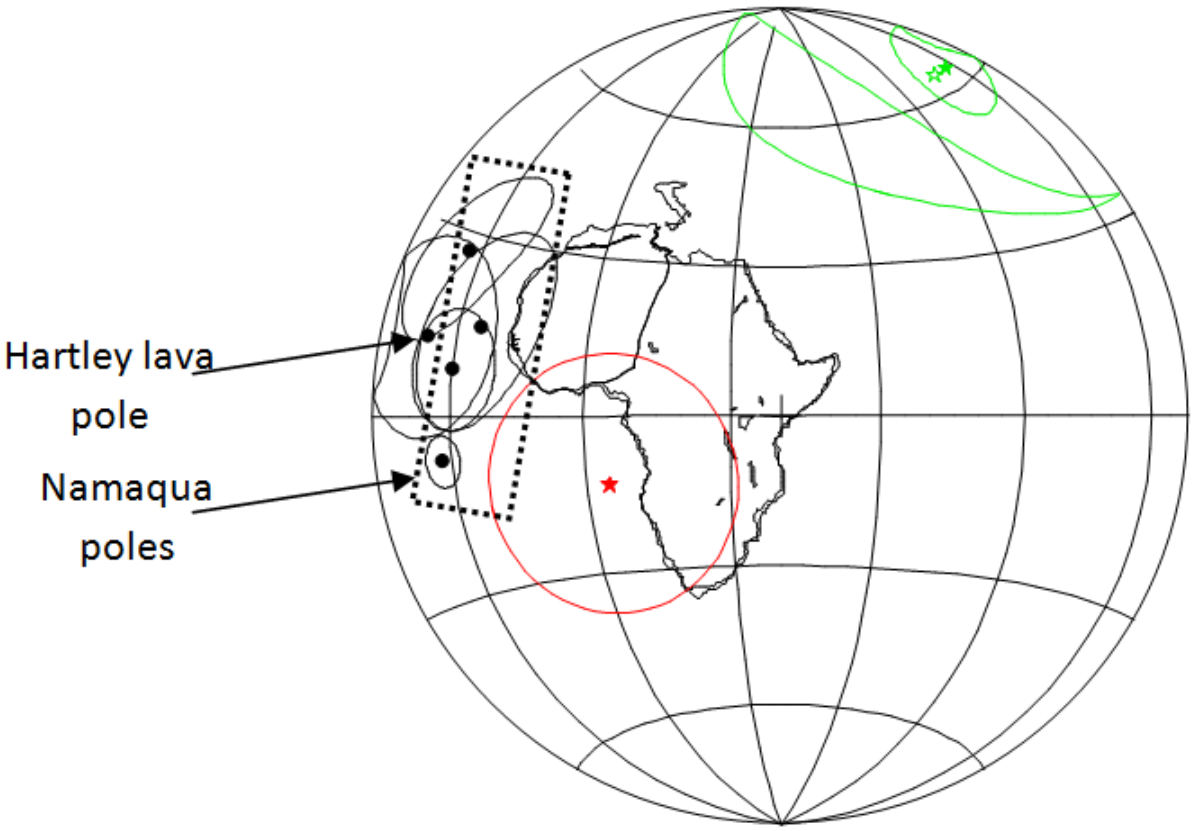

Fig. 21. Comparison of VGPs calculated for components B and C (green stars) and Component D (red star) with poles from the 1.10 Ga Namaqua-Natal Province (Pisarevsky, 2005) and 1.93 Ga Hartley Lava (Evans et al., 2002).

(1984) estimated the metamorphic peak temperature of the hosting Kuruman Formation BIF deposit to have been 170°C.

6.2.2 Primary components

Although none of the components can be shown definitively to be primary, Component E is interpreted to be so. Its corresponding VGP position (52.2° N, 93.5° E, dp = 6.2°, dm = 11.6°) does not resemble any known younger poles from southern Africa. Instead, the pole plots between the Allanridge Formation/ Rykoppies dyke swarm poles (2.7 Ga/2.66 Ga) and the Ongeluk lava/Basal Gamagara-Mapedi poles (2.22 Ga) to form part of the apparent polar wander path (Fig 21). According to the reliability criteria defined by Van der Voo (1990), a quality factor of Q = 4 for this pole can be determined, meaning that four of a total of seven quality criteria are satisfied by the dataset. These are (1) the good age determination of magnetization, (2) adequate demagnetization of samples, (3) a structural and tectonic coherence and (4) the non-resemblance of paleopoles of a younger age. One might argue that the criterion that includes both a sufficient number of samples (not met) and sufficient statistical precision (met) is partly fulfilled. However, as Component E has not been observed in more samples, I suggest treating the reliability evaluation with caution.

6.3 Implications for Vaalbara

Trendall (1968) and Button (1976) first noted similarities between the sedimentary successions and basin configurations of the Transvaal Supergroup and the Hamersley Group in the Kaapvaal and Pilbara cratons, respectively. Button (1976) concluded that the two largely coeval sedimentary successions represented spatially distinct basins, but probably shared similar depositional histories as part of a larger continental block.

Cheney et al. (1988) and Cheney (1990, 1996) pursued the idea of a common geological history of the two cratons. They suggested the possibility of a Neoarchean to Paleoproterozoic connection between the Kaapvaal and Pilbara cratons to form a supercraton which they named Vaalbara. Based on analyses of sequence stratigraphy, lithostratigraphy and lithofacies, Cheney (1990, 1996) produced a reconstruction placing Pilbara at the southern margin of Kaapvaal. This reconstruction also included the Yilgarn and Zimbabwe cratons in the delimitation of Vaalbara. Similar time-stratigraphic development is present in both Kaapvaal and Pilbara cratons. The volcanics of the Ventersdorp Supergroup and the sediments of the successive Transvaal Supergroup (Kaapvaal Craton) can be correlated with the volcanics of the Fortescue Group and the sediments of the Mount Bruce Super-

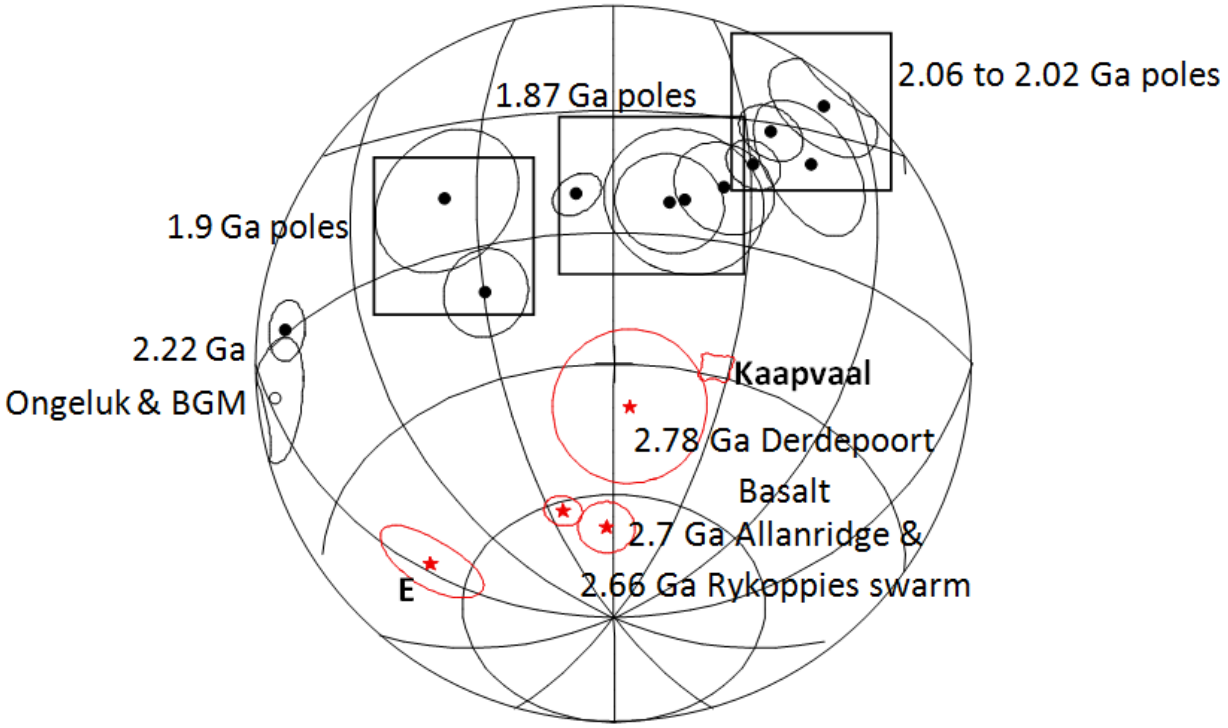

Fig. 22. Comparing component E VGP with known Neoarchean and Paleoproterozoic paleopoles from the Kaapvaal Craton. BGM = Basal Gamagara/Mapedi Formation. References of paleopoles used are as follows: 2.78 Ga Derdepoort Basalt = Wingate (1998), 2.7 Ga Allanridge Formation = De Kock et al. (2009), 2.66 Ga Rykoppies dyke swarm = Lubnina et al. (2010) (new age determination by Olsson et al., 2010), 2.22 Ga Ongeluk Lava and Basal Gamagara/Mapedi Formation = Global Paleomagnetic Database (Pisarevsky, 2005), 2.06 Ga Bushveld Complex and Palaborwa Complex = Letts et al. (2009), 1.87 Ga Bushveld and Palaborwa dykes = Letts et al. (2010), 2.054 and 1.9 Ga Waterberg Group = De Kock et al. (2006), 2.02 Ga Vredefort meteorite crater = Carporzen et al. (2005), 1.87 Ga Post-Waterberg intrusions = Hanson et al. (2004).

group (Pilbara Craton), respectively (Cheney, 1990). A comparison between similar poles of the Neoarchean Usushwana (Kaapvaal Craton) and Millindina (Pilbara Craton) complexes, as well as a correlation between Archean tectonic architecture of the respective cratons, led Zegers et al. (1998) to an alternative reconstruction with Pilbara at the eastern margin of Kaapvaal. The paleomagnetic data disproved the traditional "Cheney-fit" scenario. De Kock et al. (2009) revised paleomagnetic results for the 2.78 - 2.70 Ga interval and also presented new data from the Ventersdorp Supergroup volcanics. Based on this, a third reconstruction (herein referred to as the "De Kock-fit") places the Pilbara Craton to the northwest of the Kaapvaal Craton. The alignment of platform sediments together with the overlapping paleopoles and parallel wander paths for the 2.8 - 2.7 Ga interval favour this model. A new U-Pb baddeleyite age of ca. 2990 Ma for the Usushwana Complex (Olsson, pers. comm., 2012) also contradicts the link to the 2860 ± 20 Ma Millindina Complex (Schmidt and Embleton, 1985), thereby supporting the De Kock-fit. In addition, this suggests that the initial amalgamation of Vaalbara is likely to have occurred during the 2.8 - 2.7 Ga interval.

The Vaalbara hypothesis is corroborated by geology, geochronology and paleomagnetism until ca. 2.46 Ga (De Kock, 2007). A comparison between the latitudinal drift of the Kaapvaal and Pilbara cratons makes a 1.7 Ga connection impossible due to a northward drift of the Kaapvaal Craton and the consistent low-latitudinal position of the Pilbara Craton (De Kock, 2007). From the apparent polar wander path (APWP) reconstructions, Vaalbara is still a possible scenario at 2.0 Ga. However, the lack of a coeval and equivalent magmatic suite on the Pilbara Craton with the 2.06 Ga Bushveld Complex on the Kaapvaal Craton (Walraven et al., 1990), the largest known layered intrusion, conflicts with the Vaalbara hypothesis after 2.06 Ga (e.g. De Kock, 2007). A possible break-up scenario at 2.2 Ga is supported by the barcode match between the 2222 ± 13 Ma igneous Ongeluk Formation in the Kaapvaal Craton (Cornell et al., 1996) and 2208 ± 10 Ma volcanism in the Turee Creek Group of the Pilbara Craton (Müller et al., 2005).

Intraplate igneous events with a 2.5 - 2.4 Ga age have been identified in many cratons worldwide. Nemchin and Pidgeon (1998) determined a SHRIMP U-Pb baddeleyite age of 2418 ± 3 Ma for the Widgiemooltha dyke swarm (Yilgarn Craton, Western Australia). Söderlund et al. (2010) produced a TIMS U-Pb baddeleyite age of 2408 ± 3 Ma for the Sebanga Poort Dyke, a contemporaneous unit in Zimbabwe. Other examples include the 2440 - 2505 Ma Baltic Igneous Province of Karelian Craton, the 2505 Ma Mistassini large igneous provinces (LIP) and 2440 - 2490 Ma Matachewan LIP of Superior Craton, and the 2450 -

2500 Ma Kaminak dykes and 2480 Ma Blue Draw Gabbro of Hearne and Wyoming cratons respectively. A summary of these relevant ages is provided by Bleeker and Ernst (2006).

The previously undetermined 2442 ± 5 Ma age of the Westerberg volcanic event coincides within error with the zircon U-Pb SHRIMP age of 2449 ± 3 Ma for the Woongarra Rhyolite of the Pilbara Craton (Barley et al., 1997). This extrusive suite overlies the BIF successions of the Weeli Wolli Formation. Detrital zircons from a tuffaceous sandstone layer in the Weeli Wolli Formation yield the same age (Barley et al., 1997). Therefore, Woongarra volcanism has been interpreted as representing an LIP. There are also numerous doleritic and basaltic units within the Weeli Wolli. They are likely to reflect earlier, more basic magmatic pulses of the same LIP event and are herein suggested to be equivalent to the Westerberg dolerite sill.

Fig. 23 shows a stratigraphic column of both the Kaapvaal and Pilbara cratons of Neoarchean and Paleoproterozoic successions and includes the new age match between the Westerberg and Woongarra igneous units of this study. A common geological history during the interval between 2.8 and 2.2 Ga can be inferred.

The Woongarra Rhyolite on top of the Weeli Wolli Formation is a felsic sill unit thought to have been emplaced in two magmatic pulses (Trendall, 1995). Although a directly equivalent unit is absent in the Griqualand West Basin of Kaapvaal, there are several coeval porphyroclastic stilpnomelane pelite beds in the upper part of the Kuruman Iron Formation which are thought to be derived from felsic volcanic activity (Beukes, 1984). Tuffaceous horizons can also be found within a siliciclastic sedimentary unit in the overlying Bolgeeda Iron Formation. Zircon U-Pb dating by Gutzmer and Beukes (1998) from one of these volcanic layers yielded an age of ca. 2440 Ma.

In light of these circumstances, I suggest a major Westerberg-Woongarra LIP event to have taken place on the joined continents of Kaapvaal and Pilbara at approximately 2440 - 2450 Ma BP.

This hypothesis can be tested by paleomagnetic investigation. Using a method first introduced by Evans and Pisarevsky (2008), the great-circle arc distances between two chronologically successive paleopoles of Kaapvaal are compared with the great-circle arc distances for two coeval Pilbara poles. By locking the two landmasses in different configurations, the various age intervals can be tested for the parallelism of their polar wander paths. For the reconstruction in this study, the coeval Kaapvaal and Pilbara poles for three different ages, 2.78 Ga, ~2.7 Ga and 2.44 Ga are included (see Fig. 24 for references). The great-circle arc distances between the 2.7 Ga and 2.44 Ga poles of Kaapvaal are ca. 40° ± 16.7° if the 2.7 Ga Allanridge Lava pole is used and ca. 34° ± 15.8° if the 2.66 Ga Rykoppies dyke swarm pole is used. The coeval poles of Pilbara are ca. 21° apart. The margin of error for the individual poles allows a common and parallel wander path of the cratons and justifies the existence of Vaalbara during that time interval.

Fig. 24 illustrates two conceivable scenarios for a Vaalbara reconstruction. A continental fit similar to the previously suggested and most widely accepted reconstruction by De Kock et al. (2009) yields matching poles within error for 2.78 and 2.44 Ga, but a slight mismatch between the 2.7 Ga poles (Fig. 24a).

The reconstruction producing the statistically best fit with all three pole pairs overlapping is shown in Fig. 24b. Pilbara is situated to the northeast of Kaapvaal. It does not resemble any of the previously suggested continental configurations. Nevertheless, in this reconstruction, a Vaalbara supercraton, which accreted in the suggested 2.8 to 2.7 Ga interval, may explain extensive 2690-2560 Ma metamorphism in the Limpopo Belt of northern Kaapvaal. This metamorphic event resembles typical orogenic conditions; a clockwise P-T path, amphibolite to granulite facies overprint and peak metamorphic conditions of about 780°C and 9 - 10 kbar (Kramers et al., 2006). The Limpopo Belt also shows gradually increasing P-T conditions towards the Northern Marginal Zone (Kramers et al., 2006). A Neoarchean collision event between Kaapvaal and Pilbara could well have been responsible for this long-lived regional metamorphism.

Nonetheless, both reconstructions are based on the assumption that the 2.44 Kaapvaal paleopole (this study) and the coeval Pilbara paleopole (Evans, 2007) are of primary origin. However, there is still some uncertainty as to whether both the Woongarra volcanics pole (Evans, pers. comm., 2012) and the Westerberg sill pole are indeed primary.

Large igneous province volcanism, possibly caused by a mantle plume pushing against the crust from below, can result in rifting and significant plate movements. The most prominent example is probably the formation of the Deccan Trap LIP, which caused the rifting of India from Western Africa around 65 Ma ago. The Westerberg-Woongarra event might be responsible for triggering the break-up between Kaapvaal and Pilbara in a similar manner. Extensional tectonics and rifting result in thinning of the lithosphere and enable extensive emplacement of magma. Further support for this hypothesis is given by the gradual deepening of the basin, indicated by the shift from carbonate to BIF sedimentation in both cratons (Fig. 23).

6.4 Economic implications

A major unconformity in the vicinity of the Westerberg sill is associated with high-grade hematite iron ores that have been formed by supergene processes (Beukes et al., 2003). Significant deposits have been discovered in both the Asbestos Hills and Koegas subgroups (see Fig. 23). The unconformity postdates emplacement of the Westerberg sill. Consequently, the age obtained by this study represents a maximum age

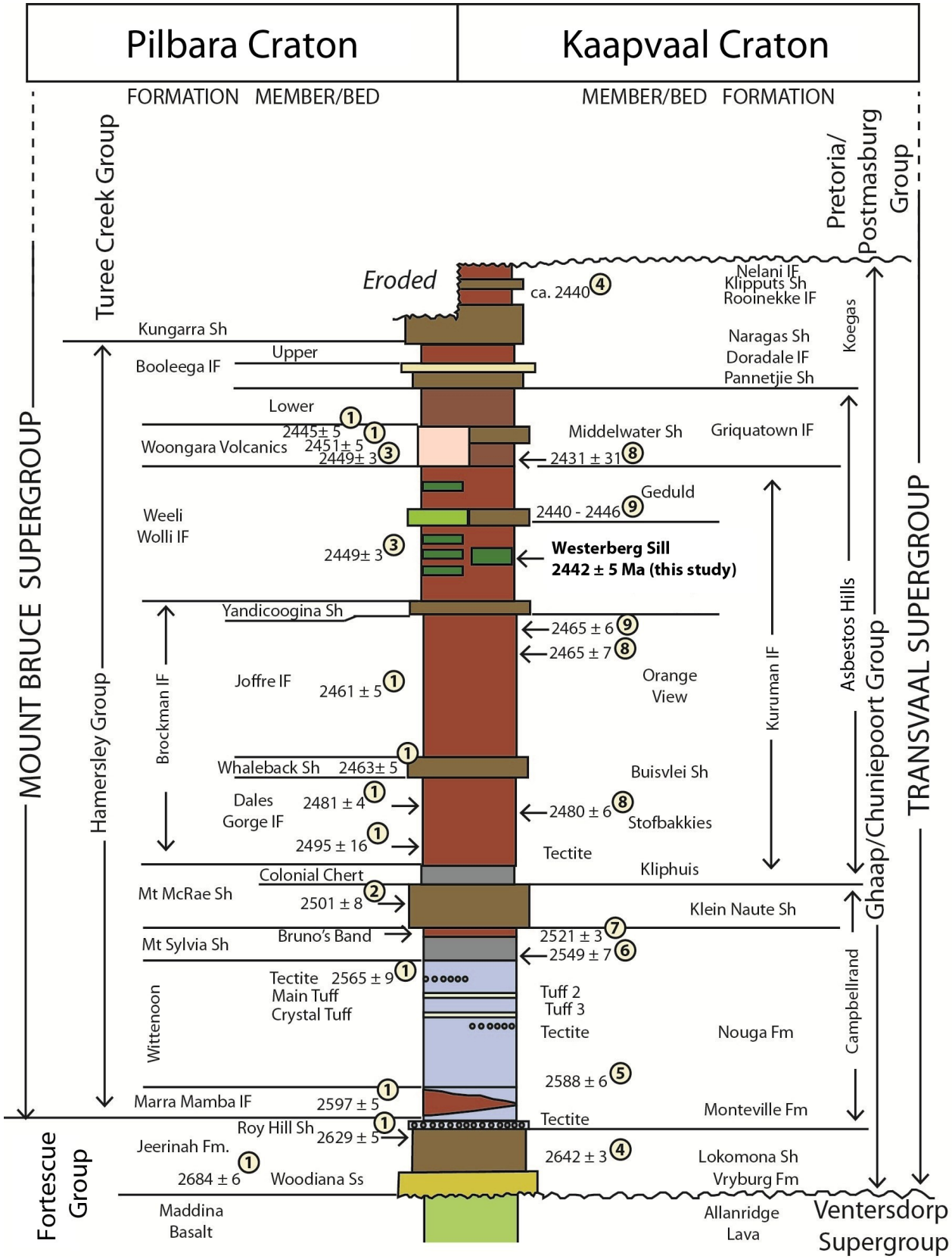

Fig. 23. Stratigraphic correlation diagram between late Neoarchean to Paleoproterozoic strata in the Transvaal and Hamersley Basins (modified after Beukes and Gutzmer, 2008), including the position and the newly obtained age data for the Westerberg sill. A shift from carbonate (light-blue) to BIF (red-brown) sedimentation at ca. 2500 Ma is also noticeable. Age references are as follows: 1 = Trendall et al. (2004), 2 = Anbar et al. (2007), 3 = Barley et al. (1997), 4 = Gutzmer and Beukes (1998), 5 = Martin et al. (1998), 6 = Alterman and Nelson (1998), 7 =Sumner and Bowring (1996), 8 = Nelson et al. (1999), 9 = Pickard (2003).

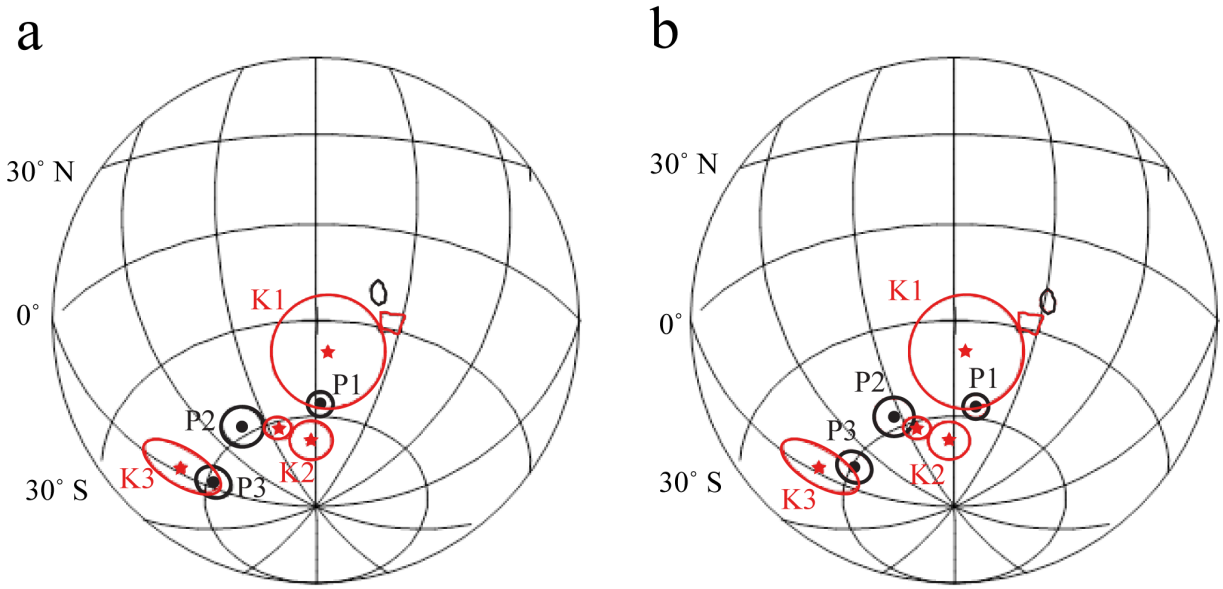

Fig. 24. Paleogeographic reconstructions of a Kaapvaal and Pilbara (Vaalbara) connection in a Kaapvaal reference frame. Great-circle arc distances: K2 (Allanridge) - K3 = 40 ± 16.7°, K2 (Rykoppies) - K3 = 34 ± 15.8°, P2 - P3 = 21 ± 11.1°. (a) Placing Pilbara to the northwest of Kaapvaal according to the most widely accepted reconstruction (De Kock et al., 2009) produces similar poles for 2.78 Ga and 2.44 Ga within 95% confidence. However, there is a mismatch for 2.7 Ga. (b) Best-fit reconstruction with all three poles overlapping within 95% confidence is achieved by placing Pilbara to the northeast of Kaapvaal. References for the Kaapvaal poles (red stars): K1 = 2782 ± 5 Ma Derdepoort Basalt (Wingate, 1998), K2 = ~2.7 Ga Allanridge Formation (De Kock et al., 2009) and 2.66 Ga Rykoppies dyke swarm (Lubnina et al., 2010), K3 = Westerberg sill (this study). References for the Pilbara poles (black dots): P1 = 2772 ± 2 Ma Pilbara Flood basalt Package 1 (Strik et al., 2003), P2 = 2717 ± 2 Ma Pilbara Flood basalt Package 8-10 (Strik et al., 2003), P3 = 2449 ± 3 Ma Woongarra Rhyolite (Evans, 2007; Evans, pers. comm., 2012).

7 Conclusion

- Baddeleyite U-Pb dating of the Westerberg sill near the SW margin of the Kaapvaal Craton yields an age of 2442 ± 5 Ma. The mafic subvolcanic unit can be correlated with the coeval Woongarra volcanics of the Pilbara Craton to form a Westerberg-Woongarra large igneous province.

- Paleomagnetic investigation and the comparison to coeval Pilbara poles allows for Vaalbara (Kaapvaal-Pilbara) reconstructions, placing Pilbara to the north of Kaapvaal in a Kaapvaal reference frame.

- In addition to geochronology and paleomagnetism, the link between the cratons is also supported by geology, reinforcing the existence of Vaalbara as well as its persistence into the Paleoproterozoic. The Westerberg-Woongarra volcanic event might have been responsible for the break-up of Vaalbara.

8 Acknowledgements

I feel highly indepted to my two supervisors, Ulf Söderlund and Michiel de Kock, for suggesting this wonderful project and helping me finding my way in the field, in the labs and in the writing process. The staff and students of the Department of Geology at the University of Johannesburg are acknowledged for the warm welcome and great hospitality I enjoyed during my stay in South Africa. I also want to thank Leif Johansson for helping me with the grain polishing and the SEM lab. Johan Olsson supported me a lot with both insightful comments and fruitful discussions. Many figures and also parts of the text were significantly improved thanks to reviews by Kursat Demirer. Finally, I would like to express my deepest gratitude towards my family. I have always felt your unconditional support and encouragement, independent of the growing geographic distance between us. This work and all my previous studies would not have been possible without you.

9 References

Altermann, W., Hälbich, I.W., 1990. Thrusting, folding and stratigraphy of the Ghaap Group along the southwestern margin of the Kaapvaal Craton. South African Journal of Geology 93, 553-566.

Altermann, W., Nelson, D.R., 1998. Sedimentation rates, basin analysis and regional correlation of three Neoarchean and Paleoproterozoic sub-

basins of the Kaapvaal craton as implied by precise SHRIMP U-Pb zircon ages from volcanic sediments. Journal of Sedimentary Geology 120, 225-256.

Anbar, A.D., Duan, Y., Lyons, T.W., Arnold, G.L., Kendal, B., Creaser, R.A., Kaufman, A.J., Gordon, G.W., Scott, C., Gavin, J., Buick, R., 2007. A whiff of oxygen before the great oxidation event? Science 317, 1903-1906.

Barley, M.E., Pickard, A.L., Sylvester, P.J., 1997. Emplacement of a large igneous province as a possible cause of a banded iron formation 2.45 billion years ago. Nature 385, 55-58.

Beukes, N.J., 1984. Sedimentology of the Kuruman and Griquatown Iron-formations, Transvaal Supergroup, Griqualand West, South Africa. Precambrian Research 24, 47-84.

Beukes, N.J., Gutzmer, J., 2008. Origin and paleoenvironmental significance of major iron formations at the Archean-Paleoproterozoic boundary. Society of Economic Geologists Reviews 15, 5-47.

Beukes, N.J., Gutzmer, J., Mukhopadhyay, J., 2003. The geology and genesis of high-grade hematite iron ore deposits. Applied Earth Science (Trans. Inst. Min. Metall B) 112, 19-25.

Bleeker, W., 2003. The late Archean record: a puzzle in ca. 35 pieces. Lithos 71, 99-134.

Bleeker, W., Ernst, R., 2006. Short-lived mantle generated magmatic events and their dyke swarms: The key unlocking Earth's paleogeographic record back to 2.6 Ga. In: Hanski, E., Mertanen, S., Ramö, T., Vuollo, J. (Eds.), Dyke Swarms – Time Markers of Crustal Evolution. Taylor and Francis, London, pp. 3-26.

Brandl, G., Cloete, M., Anhaeusser, C.R., 2006. Archean Greenstone Belts. In Johnson, M.R., Anhaeusser, C.R., Thomas, R.J. (Eds.), The Geology of South Africa. Geological Society of South Africa, Johannesburg, pp. 9-56.

Buchan, K.L., Le Cheminant, A.N., van Breemen, O., 2009. Paleomagnetism and U-Pb geochronology of the Lac de Gras diabase dyke swarm, Slave Province, Canada: Implications for relative drift of Slave and Superior provinces in the Paleoproterozoic. Canadian Journal of Earth Sciences 46, 361-379.

Bumby, A.J., Eriksson, P.G., Catuneanu, O., Nelson, D.R., Rigby, M.J., 2011. Meso-Archean and paleo-proterozoic sedimentary sequence stratigraphy of the Kaapvaal Craton. Marine and Petroleum Geology, doi: 10/1016/ j.marpetgeo.2011.09.010.

Button, A., 1976. Transvaal and Hamersley Basins -- review of basin development and mineral deposits. Minerals Science and Engineering 8, 262-290.

Carporzen, L., Gilder, S.A., Hart, R.J., 2005. Palaeomagnetism of the Vredefort meteorite crater and implications for craters in Mars. Nature 435, 198-201.

Cheney, E.S., 1990. Evolution of the "Southwestern" continental margin of Vaalbara. Extended Abstracts Geocongress '90, Geological Society of South Africa, Cape Town, 88-91.

Cheney, E.S., 1996. Sequence stratigraphy and plate tectonic significance of the Transvaal succession of southern Africa and its equivalent in Western Australia. Precambrian Research 79, 3-24.

Cheney, E.S., Roering, C., Stettler, E., 1988. Vaalbara. Extended Abstracts of Geocongress '88, Geological Society of South Africa, Durban, 85-88.

Cogné, J.P., 2003. PaleoMac: A Macintosh application for reconstructions. Geochemistry Geophysics Geosystems 4, 1007.

Cornell, D.H., Armstrong, R.A., Walraven, F., 1998. Geochronology of the Hartley Formation, South Africa: constraints on the Kheis tectogenesis and the Kaapvaal Craton's earliest Wilson cycle. Journal of African Earth Sciences 26, 5-27.

Cornell, D.H., Schütte, S.S., Eglington, B.L., 1996. The Ongeluk Basaltic Andesite Formation in Griqualand West, South Africa: submarine alteration in a 2222 Ma Proterozoic sea. Precambrian Research 79, 101-124.

Crow, C., Condie, K.C., 1988. Geochemistry and origin of late Archean volcanics from the Ventersdorp Supergroup, South Africa. Precambrian Research 42, 19-37.

De Kock, M.O., 2007. Paleomagnetism of selected Neoarchean-Paleoproterozoic Cover sequences on the Kaapvaal Craton and implications for Vaalbara. PhD thesis, The University of Johannesburg, Johannesburg, South Africa, 276 pp.

De Kock, M.O., Evans, D.A.D., Beukes, N.J., 2009. Validating the existence of Vaalbara in the Neoarchean. Precambrian Research 174, 145-154.

De Kock, M.O., Evans, D.A.D., Dorland, H.C., Beukes, N.J., Gutzmer, J., 2006. Paleomagnetism of the lower two unconformity-bounded sequences of the Waterberg Group, South Africa: Towards a better defined apparent polar wander path for the Paleoproterozoic Kaapvaaal Craton. South African Journal of Geology 109, 157-182.

Dreyer, C.J.B., 1982. Amphibole Asbestos in South Africa. PhD thesis, Rand Afrikaans University, Johannesburg, South Africa, 301 pp.

Eales, H.V., Cawthorn, R.G., 1996. The Bushveld Complex. Developments in Petrology 15, 181-229.

Eglington, B.M., 2006. Evolution of the Namaqua-Natal Belt, southern Africa - A geochronological and isotope geochemical review. Journal of African Earth Sciences 46, 93-111.

Eglington, B.M., Armstrong, R.A., 2004. The Kaapvaal Craton and adjacent orogens, South Africa: a geochronological database and overview of the geological development of the craton. South African Journal of Geology 107, 13-32.

Eriksson, P.G., Altermann, W., Hartzer, F.J., 2006. The Transvaal Supergroup and its precursors. In Johnson, M.R., Anhaeusser, C.R., Thomas, R.J. (Eds.), The Geology of South Africa. Geological Society of South Africa, Johannesburg, pp. 237-260.

Evans, D.A.D., 2007. Key Paleomagnetic pole from the Woongarra / Weeli Wolli large igneous province, Pilbara Craton, Australia: A link between supercratons? Geological Society of America Abstracts with Programs 39, 285.

Evans, D.A.D., Beukes, N.J. and Kirschvink, J.L., 2002. Palaeomagnetism of a lateritic paleoweathering horizon and overlying Paleoproterozoic red beds from South Africa: Implications for the Kaapvaal apparent polar wander path and a confirmation of atmospheric oxygen enrichment. Journal of Geophysical Research 107, doi:10.1029/2001JB000432.

Evans, D.A.D., Halls, H.C., 2010. Restoring Proterozoic deformation within the Superior Craton. Precambrian Research 183, 474-489.

Evans, D.A.D., Pisarevsky, S.A., 2008. Plate tectonics on the early Earth?- weighing the paleomagnetic evidence. In: Condie, K., Pease, V. (Eds.), When did Plate Tectonics Begin? Geological Society of America, pp. 249-263.

Gnos, E., Armbruster, T., Villa, I.M., 2003. Norrishite, $K(Mn_2^{3+}Li)Si_4O_{10}(O)_2$, an oxymica associated with sugilite from the Wessels Mine, South Africa: Crystal chemistry and ^{40}Ar-^{39}Ar dating. American Mineralogist 88, 189-194.

Gutzmer, J., Beukes, N.J., 1998. High-grade manganese ores in the Kalahari manganese field: Characterization and dating of the ore forming events. Unpublished Report, Rand Afrikaans University, Johannesburg, South Africa, 221 pp.

Hanson, R.E., Gose, W.A., Crowley, J., Ramezani, S.A., Bowring, D.S., Hall, R.P., Pancake, J.A., Mukwakwami, J., 2004. Paleoproterozoic intraplate magmatism and basin development on the Kaapvaal Craton: age, paleomagnetism and geochemistry of ~1.93 to ~1.87 Ga post-Waterberg dolerites. South African Journal of Geology 107, 233-254.

Jaffey, A.H., Flynn, K.F., Glendenin, L.E., Bentley, W.C., Essling, A.M., 1971. Precision measurements of half-lives and specific activities of ^{235}U and ^{238}U. Physical Reviews 4, 1889-1906.

Jones, C.H., 2002. User-driven integrated software lives: "Paleomag" Paleomagnetic analysis on the Macintosh™. Computers and Geosciences 28, 1145-1151.

Keyser, N., 1997. Geological map of the Republic of South Africa and the Kingdoms of Leshoto and Swaziland, Council for Geoscience, Pretoria, 1:1 000 000.

Kirschvink, J.L., 1980. The least squares line and plane and the analysis of paleomagnetic data. Geophysical Journal of the Royal Astronomical Society 62, 699-718.

Kramers, J.D., McCourt, S., van Reenen, D.D., 2006. The Limpopo Belt. In Johnson, M.R., Anhaeusser, C.R., Thomas, R.J. (Eds.), The Geology of South Africa. Geological Society of South Africa, Johannesburg, pp. 209-236.

Letts, S., Torsvik, T.H., Webb, S.J., Ashwal, L.D., 2009. Paleomagnetism of the 2054 Ma Bushveld Complex (South Africa): Implications for emplacement and cooling. Geophysical Journal International 179, 850-872.

Letts, S., Torsvik, T.H., Webb, S.J., Ashwal, L.D., 2010. New Palaeoproterozoic palaeomagnetic data from the Kaapvaal Craton, South Africa. Geological Society, London, Special Publications 357, 9-26.

Lubnina, N., Ernst, R.E., Klausen, M., Söderlund, U., 2010. Paleomagnetic study of Neoarchean-Paleoproterozoic dykes in the Kaapvaal Craton. Precambrian Research 183, 523-552.

Ludwig, K.R., 2003. Isoplot 3.00: A geochronological toolkit for Microsoft Excel. Berkeley Geochronology Center Special Publication 2003, 1-70.

Malherbe, S.J., Moen, H.F.G., 1996. Geological map 2922 Prieska, Department of Mines, South Africa, 1:250000.

Martin, D.M., Clenednin, C.W., Krapez, B., Mcnaughton, N.J., 1998. Tectonic and geochronological constraints on Late Archaean and Palaeoproterozoic stratigraphic correlation within and between the Kaapvaal and Pilbara cratons. Journal of the Geological Society of Australia 155, 311-322.

Mccarthy, T.S., 2006. The Witwatersrand Supergroup. In Johnson, M.R., Anhaeusser, C.R., Thomas, R.J. (Eds.), The Geology of South Africa. Geological Society of South Africa, Johannesburg, 237-260.

Miyano, T., Beukes, N.J., 1984. Phase relations of stilpnomelane, ferri-annite, and riebeckite in very low-grade metamorphosed iron-formations. Transactions of the Geological Society of South Africa 87, 111-124.

Moyen, J., van Hunen, J., 2012. Short-term episodicity of Archaean plate tectonics. Geology 40, 451-454.

Müller, S.G., Krapez, B., Barley, M.E., Fletcher, I.R., 2005. Giant ore-deposits oft he Hamersley province related tot he breakup of Paleoproterozoic Australia: New insights from in situ SHRIMP dating of baddeleyite from mafic intrusions. Geology 33, 577-580.

Næraa, T., Scherstén, A., Rosing, M.T., Kemp, A.I.S., Hoffmann, J.E., Kokfeldt, T.F., Whitehouse, M.J., 2012. Hafnium isotope evidence for a transition in the dynamics of continental growth 3.2 Gyr ago. Nature 485, 627-630.

Nelson, D.R., Trendall, A.F., Altermann, W., 1999. Chronological correlations between the Pilbara

and Kaapvaal Cratons. Precambrian Research 97, 165-189.

Nemchin, A.A., Pidgeon, R.T., 1998. Precise conventional and SHRIMP baddeleyite U-Pb age for the Binneringie Dyke, near Narrogin, Western Australia. Australian Journal of Earth Sciences 45, 673-675.

Olsson, J.R., Söderlund, U., Klausen, M.B., Ernst, R.E., 2010. U-Pb baddeleyite ages linking major Archean dyke swarms to volcanic-rift forming events in the Kaapvaal Craton (South Africa), and a precise age for the Bushveld Complex. Precambrian Research 183, 490-500.

Partridge, T.C., Botha, G.A., Haddon, I.G., 2006. Cenozoic deposits of the interior. In Johnson, M.R., Anhaeusser, C.R., Thomas, R.J. (Eds.), The Geology of South Africa. Geological Society of South Africa, Johannesburg, 585-604.

Pickard, A.L., 2003. SHRIMP U-Pb zircon ages for the Palaeoproterozoic Kuruman Iron Formation, northern Cape Province, South Africa: Evidence for simultaneous BIF deposition on Kaapvaal and Pilbara cratons. Precambrian Research 125, 275-315.

Pisarevsky, S.A., 2005. New edition of the Paleomagnetic Database. Eos Transactions of the American Geophysical Union 86, 170.

Schmidt, P.W., Embleton, B.J.J., 1985. Prefolding and overprint magnetic signatures in Precambrian (~2.9 to 2.7 Ga) igneous rocks from the Pilbara Craton and Hamersley Basin, N.W. Australia. Journal of Geophysical Research 90, 2967-2984.

Scoates, J.S., Friedman, R.M., 2008. Precise age of the platiniferous Merensky Reef, Bushveld Complex, South Africa, by the U-Pb zircon chemical abrasion ID-TIMS technique. Economic Geology 103, 465-471.

Söderlund, U., 1996. Conventional U-Pb dating versus single-grain Pb evaporation dating of complex zircons from a pegmatite in the high-grade gneisses of southwestern Sweden. Lithos 38, 93-105.

Söderlund, U., Hofmann, A., Klausen, M.B., Olsson, J.R., Ernst, R.E., Persson, P.-E., 2010. Towards a complete magmatic barcode for the Zimbabwe craton: Baddeleyite U–Pb dating of regional dolerite dyke swarms and sill complexes. Precambrian Research 183, 388-398.

Söderlund, U., Johansson, L., 2002. A simple way to extract baddeleyite (ZrO_2). Geochemistry Geophysics Geosystems 3, 1014, doi: 10.1029/2001GC000212.

Spry, A., 1962. The origin of columnar jointing, particularly in basalt flows. Journal of the Australian Geological Society 8, 192-216.

Stacey, J.S., Kramers, J.D., 1975. Approximation of Terrestrial Lead Isotope Evolution by a 2-Stage Model. Earth and Planetary Science Letters 26, 207-221.

Strik, G., Blake, T.S., Zegers, T.E., White, S.H., Langereis, C.G., 2003. Paleomagnetism of flood basalt in the Pilbara Craton, Western Australia: Late Archean continental drift and the oldest known reversal of the geomagnetic field. Journal of Geophysical Research 108, doi: 10.1029/2003JB002475.

Sumner, D.Y., Bowring, S.A., 1996. U-Pb geochronologic constraints on deposition of the Campbellrand Subgroup, Transvaal Supergroup, South Africa. Precambrian Research 78, 25-35.

Tauxe, L., Butler, R.F., Van der Voo, R., Banerjee, S.K., 2010. Essentials of paleomagnetism. University of California Press, Berkeley.

Trendall, A.F., 1968. Three great basins of Precambrian iron formation deposition: a systematic comparison. Geological Society of America Bulletin 79, 1527-1533.

Trendall, A.F., 1995. The Woongarra Rhyolite – a giant lava-like felsic sheet in the Hamersley Basin of Western Australia. Geological Survey of Western Australia Report 42, 70 pp.

Trendall, A.F., Compston, W., Nelson, D.R., De Laeter, J.R., Bennet, V.C., 2004. SHRIMP zircon ages constraining the depositional chronology of the Hamersley Group, Western Australia. Australian Journal of Earth Sciences 51, 621-644.

Trendall, A.F., Compston, W., Williams, I.S., Armstrong, R.A., Arndt, N.T., McNaughton, N.J., Nelson, D.R., Barley, M.E., Beukes, N.J., De Laeter, J.R., Retief, E.A., Thorne, A.M., 1990. Precise zircon U-Pb chronological comparison of the volcano-sedimentary sequences of the Kaapvaal and Pilbara Cratons between about 3.1 and 2.4 Ga. Abstracts of the Third International Association of Sedimentologis Conference, Perth, 81-83.

Trendall, A.F., De Laeter, J.R., Nelson, D.R., 1995. Chronology of Gondwana BIFs: progress report from recent zircon U-Pb results. Abstracts of the Third Australian Conference of Geochronology, 1-3.

Van der Voo, R., 1990. The reliability of paleomagnetic data. Tectonophysics 184, 1-9.

Van der Westhuizen, W.A., De Bruiyn, H., Meintjes, P.G., 2006. The Ventersdorp Supergroup. In Johnson, M.R., Anhaeusser, C.R., Thomas, R.J. (Eds.), The Geology of South Africa. Geological Society of South Africa, Johannesburg, pp. 187-208.

Walraven, F., 1997. Geochronology of the Rooiberg Group, Transvaal Supergroup, South Africa. Economic Geology Research Unit Information Circular 316, University of the Witwatersrand, Johannesburg, 21 pp.

Walraven, F., Armstrong, R.A., Kruger, F.J., 1990. A chronostratigraphic framework for the north-central Kaapvaal Craton, the Bushveld Complex

and Vredefort structure. Tectonophysics 171, 23-48.

Walraven, F., Martini, J., 1995. Zircon Pb-evaporation age determinations of the oak tree formation, Chuniespoort group, Transvaal sequence: implications for Transvaal-Griqualand west basin correlations. South African Journal of Geology 98, 58-67.

Wingate, M.T.D., 1998. A paleomagnetic test of the Kaapvaal-Pilbara (Vaalbara) connection at 2.78 Ga. South African Journal of Geology 101, 257-274.

Zegers, T.E., de Wit, M.J., Dann, J., White, S.H., 1998. Vaalbara, Earth's oldest assembled continent? A combined structural, geochronological and palaeomagnetic test. Terra Nova 10, 250-259.

Tidigare skrifter i serien ”Examensarbeten i Geologi vid Lunds Universitet”:

265. Petersson, Andreas, 2010: Zircon U-Pb, Hf and O isotope constraints on the growth versus recycling of continental crust in the Grenville orogen, Ohio, USA. (45 hskp)
266. Stenberg, Li, 2010: Geophysical and hydrogeological survey in a part of the Nhandugue River valley, Gorongosa National Park, Mozambique – Area 1 and 2. (45 hskp)
267. Andersen, Christine, 2010: Controls of seafloor depth on hydrothermal vent temperatures - prediction, observation & 2D finite element modeling. (45 hskp)
268. März, Nadine, 2010: When did the Kalahari craton form? Constraints from baddeleyite U-Pb geochronology and geo-chemistry of mafic intrusions in the Kaapvaal and Zimbabwe cratons. (45 hp)
269. Dyck, Brendan, 2010: Metamorphic rocks in a section across a Svecnorwegian eclogite-bearing deformation zone in Halland: characteristics and regional context. (15 hp)
270. McGimpsey, Ian, 2010: Petrology and lithogeochemistry of the host rocks to the Nautanen Cu-Au deposit, Gällivare area, northern Sweden. (45 hp)
271. Ulmius, Jan, 2010: Microspherules from the lowermost Ordovician in Scania, Sweden – affinity and taphonomy. (15 hp)
272. Andersson, Josefin, Hybertsen, Frida, 2010: Geologi i Helsingborgs kommun – en geoturistkarta med beskrivning. (15 hp)
273. Barth, Kilian, 2011: Late Weichselian glacial and geomorphological reconstruction of South-Western Scania, Sweden. (45 hp)
274. Mashramah, Yaser, 2011: Maturity of kerogen, petroleum generation and the application of fossils and organic matter for paleotemperature measurements. (45 hp)
275. Vang, Ina, 2011: Amphibolites, structures and metamorphism on Flekkerøy, south Norway. (45 hp)
276. Lindvall, Hanna, 2011: A multi-proxy study of a peat sequence on Nightingale Island, South Atlantic. (45 hp)
277. Bjerg, Benjamin, 2011: Metodik för att förhindra metanemissioner från avfallsdeponier, tillämpad vid Albäcksdeponin, Trelleborg. (30 hp)
278. Pettersson, Hanna, 2011: El Hicha – en studie av saltstäppssediment. (15 hskp)
279. Dyck, Brendan, 2011: A key fold structure within a Sveconorwegian eclogite-bearing deformation zone in Halland, south-western Sweden: geometry and tectonic implications. (45 hp)
280. Hansson, Anton, 2011: Torvstratigrafisk studie av en trädstamshorisont i Viss mosse, centrala Skåne kring 4 000 - 3 000 cal BP med avseende på klimat- och vattenståndsförändringar. (15 hp)
281. Åkesson, Christine, 2011: Vegetationsutvecklingen i nordvästra Europa under Eem och Weichsel, samt en fallstudie av en submorän, organisk avlagring i Bellinga stenbrott, Skåne. (15 hp)
282. Silveira, Eduardo M., 2011: First precise U-Pb ages of mafic dykes from the São Francisco Craton. (45 hp)
283. Holm, Johanna, 2011**:** Geofysisk utvärdering av grundvattenskydd mellan väg 11 och Vombs vattenverk. (15 hp)
284. Löfgren, Anneli, 2011: Undersökning av geofysiska metoders användbarhet vid kontroll av den omättade zonen i en infiltrationsdamm vid Vombverket. (15 hp)
285. Grenholm, Mikael, 2011: Petrology of Birimian granitoids in southern Ghana - petrography and petrogenesis. (15 hp)
286. Thorbergsson, Gunnlaugur, 2011: A sedimentological study on the formation of a hummocky moraine at Törnåkra in Småland, southern Sweden. (45 hp)
287. Lindskog, Anders, 2011: A Russian record of a Middle Ordovician meteorite shower: Extraterrestrial chromite in Volkhovian-Kundan (lower Darriwilian) strata at Lynna River, St. Petersburg region. (45 hp)
288. Gren, Johan, 2011: Dental histology of Cretaceous mosasaurs (Reptilia, Squamata): incremental growth lines in dentine and implications for tooth replacement. (45 hp)
289. Cederberg, Julia, 2011: U-Pb baddelyit dateringar av basiska gångar längs Romeleåsen i Skåne och deras påverkan av plastisk deformation i Protoginzonen (15 hp)
290. Ning, Wenxing, 2011: Testing the hypothesis

of a link between Earth's magnetic field and climate change: a case study from southern Sweden focusing on the 1st millennium BC. (45 hp)

291. Holm Östergaard, Sören, 2011: Hydrogeology and groundwater regime of the Stanford Aquifer, South Africa. (45 hp)
292. Tebi, Magnus Asiboh, 2011: Metamorphosed and partially molten hydrothermal alteration zones of the Akulleq glacier area, Paamiut gold province, South-West Greenland. (45 hp)
293. Lewerentz, Alexander, 2011: Experimental zircon alteration and baddeleyite formation in silica saturated systems: implications for dating hydrothermal events. (45 hp)
294. Flodhammar, Ingrid, 2011: Lövestads åsar: En isälvsavlagring bildad vid inlandsisens kant i Weichsels slutskede. (15 hp)
295. Liu, Tianzhuo, 2012: Exploring long-term trends in hypoxia (oxygen depletion) in Western Gotland Basin, the Baltic Sea. (45 hp)
296. Samer, Bou Daher, 2012: Lithofacies analysis and heterogeneity study of the subsurface Rhaetian–Pliensbachian sequence in SW Skåne and Denmark. (45 hp)
297. Riebe, My, 2012: Cosmic ray tracks in chondritic material with focus on silicate mineral inclusions in chromite. (45 hp)
298. Hjulström, Joakim, 2012: Återfyllning av borrhål i geoenergisystem: konventioner, metod och material. (15 hp)
299. Letellier, Mattias, 2012: A practical assessment of frequency electromagnetic inversion in a near surface geological environment. (15 hp)
300. Lindenbaum, Johan, 2012: Identification of sources of ammonium in groundwater using stable nitrogen and boron isotopes in Nam Du, Hanoi. (45 hp)
301. Andersson, Josefin, 2012: Karaktärisering av arsenikförorening i matjordsprofiler kring Klippans Läderfabrik. (45 hp)
302. Lumetzberger, Mikael, 2012: Hydrogeologisk kartläggning av infiltrationsvattentransport genom resistivitetsmätningar. (15 hp)
303. Martin, Ellinor, 2012: Fossil pigments and pigment organelles – colouration in deep time. (15 hp)
304. Rådman, Johan, 2012: Sällsynta jordartsmetaller i tungsand vid Haväng på Österlen. (15 hp)
305. Karlstedt, Filippa, 2012: Jämförande geokemisk studie med portabel XRF av obehandlade och sågade ytor, samt pulver av Karlshamnsdiabas. (15 hp)
306. Lundberg, Frans, 2012: Den senkambriska alunskiffern i Västergötland – utbredning, mäktigheter och faciestyper. (15 hp)
307. Thulin Olander, Henric, 2012: Hydrogeologisk kartering av grundvattenmagasinet Ekenäs-Kvarndammen, Jönköpings län. (15 hp)
308. Demirer, Kursad, 2012: U-Pb baddeleyite ages from mafic dyke swarms in Dharwar craton, India – links to an ancient supercontinent. (45 hp)
309. Leskelä, Jari, 2012: Loggning och återfyllning av borrhål – Praktiska försök och utveckling av täthetskontroll i fält. (15 hp)
310. Eriksson, Magnus, 2012: Stratigraphy, facies and depositional history of the Colonus Shale Trough, Skåne, southern Sweden. (45 hp)
311. Larsson, Amie, 2012: Kartläggning, beskrivning och analys av Kalmar läns regionalt viktiga vattenresurser. (15 hp)
312. Olsson, Håkan, 2012: Prediction of the degree of thermal breakdown of limestone: A case study of the Upper Ordovician Boda Limestone, Siljan district, central Sweden. (45 hp)
313. Kampmann, Tobias Christoph, 2012: U-Pb geochronology and paleomagnetism of the Westerberg sill, Kaapvaal Craton – support for a coherent Kaapvaal-Pilbara block (Vaalbara). (45 hp)

LUNDS UNIVERSITET

Geologiska institutionen
Lunds universitet
Sölvegatan 12, 223 62 Lund